

Planet-Detection Simulations for Several Possible TESS Extended Missions

Luke Bouma, Josh Winn, Jacobi Kosiarek, Peter McCullough

October 29, 2016

Executive Summary

The Transiting Exoplanet Survey Satellite (*TESS*) will perform a two-year, nearly all-sky survey for transiting exoplanets. There do not appear to be any fundamental obstacles to continuing science operations for at least several years after this Primary Mission. Any Extended Mission will likely need to be organized while the Primary Mission is occupying most of the *TESS* team's attention. The purpose of this Memo, and the accompanying Wiki document¹ is to provide a head start to those who are planning and proposing for an Extended Mission.

The choice of an Extended Mission is likely to be influenced by many factors besides the prospects for planet detection. We have created a freely editable document on the *TESS* wiki to raise and discuss those broad issues. This Memo is narrowly focused on planet detection. Using Monte Carlo simulations, we try to anticipate the quantities and types of planets that would be detected during several plausible scenarios for a one-year Extended Mission following the two-year Primary Mission. Our main focus is on strategies for scanning the sky. For simplicity we do not compare different choices either for the cadence of photometric measurements or for the target stars to be selected, although different choices might prove to be advantageous and should be studied in future work.

Throughout this report we consider six different scenarios for Year 3 of the *TESS* mission, illustrated in Figure 1:

1. *hemi*, which re-observes one of the ecliptic hemispheres in essentially the same manner as in the Primary Mission (i.e., neglecting the zone within 6° of the ecliptic);
2. *hemi+ecl*, which re-observes one of the ecliptic hemispheres, but this time covering the entire hemisphere at the expense of the continuous-viewing zone near the pole;
3. *pole*, which focuses on one of the two ecliptic poles;
4. *ecl_long*, which has a series of pointings with the long axis of the $24^\circ \times 96^\circ$ field-of-view along the ecliptic (in combination with some fields near the ecliptic pole, when the Earth or Moon would prevent effective observations of the ecliptic);
5. *ecl_short*, which has a series of pointings with the short axis of the field-of-view along the ecliptic (again in combination with some fields near the ecliptic pole);
6. *allsky*, which covers nearly the entire sky with 14-day pointings (as opposed to the 28-day pointings of the Primary Mission), by alternating between northern and southern hemispheres.

¹ <https://spacebook.mit.edu/display/TESS/Extended+Missions>. Contact luke@astro.princeton.edu, copying imeister@mit.edu, for an account with editing rights.

We numerically compute the results based on the methodology of Sullivan et al. [2015], after bug fixes and enhancements by Luke Bouma in consultation with Josh Winn. Additional inputs were provided by Jacobi Kosiarek and Peter McCullough.

Some of the most important findings are:

1. The overall quantity of detected planets does not depend strongly on the sky-scanning schedule. Among the six scenarios considered here, the number of newly-detected sub-Neptune planets is the same to within about 30%.
2. The number of newly-detected sub-Neptune planets in Year 3 is approximately the same as the number detected in either Year 1 or Year 2. Thus, we do not expect a sharp fall-off in the planet discovery rate in Year 3. This is because the Primary Mission will leave behind many short-period transiting planets with bright host stars, with a signal-to-noise ratio just below the threshold for detection. These planets can be detected by collecting more data in Year 3.
3. Regarding newly detected sub-Neptunes, the `allsky`, `pole`, and `hemi+ecl` strategies offer the greatest number (1300–1400, as compared to the 1250 during each year of the Primary Mission).
4. Regarding planets with orbital periods >20 days, the `allsky`, `pole`, and `hemi` strategies would discover twice as many such planets as will be discovered in each year of the Primary Mission. This would help to overcome one of the main limitations of the Primary Mission: the strong bias toward shorter orbital periods.
5. Regarding new planets with very bright host stars ($I_c < 10$), the `allsky`, `hemi+ecl`, and `ecl_short` strategies offer the greatest num-

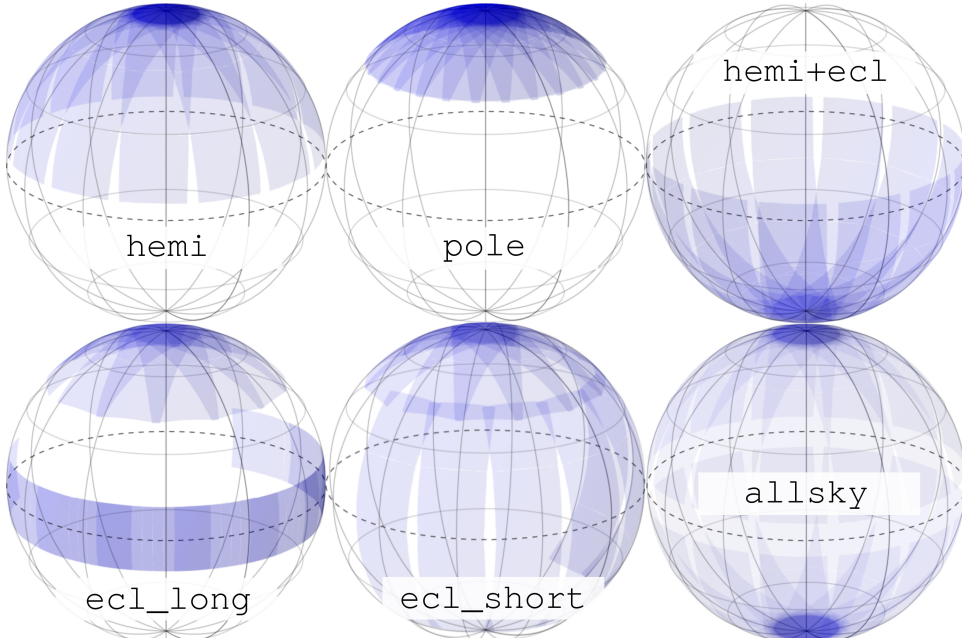


Figure 1: Six proposed pointing strategies for a *TESS* Extended Mission, visualized in ecliptic coordinates. Note that none of these scenarios spend the entire year observing the ecliptic; we concluded that such a plan would be inadvisable because of interruptions by the Earth and Moon (see Fig. 9).

bers (~ 190 , about the same as are found in each year of the Primary Mission; see Table 2).

6. Regarding planets with near-terrestrial insolation ($0.2 < S/S_{\oplus} < 2$), all the strategies considered here offer similar numbers (about 120, as compared to 105 in each year of the Primary Mission).
7. Apart from detecting new planets, a potentially important function of an Extended Mission would be to improve our ability to predict the times of future transits and eclipses of *TESS*-detected planets. With data from the Primary Mission alone, the uncertainty in transit ephemerides will inhibit follow-up observations after only a few years.

The rest of this report is organized as follows. Sec. 1 discusses how we selected and compared different pointing strategies, as well as how we modeled *TESS*'s observations and planet detections. Sec. 1.7 gives a list of the most important assumptions we made for the simulations. Sec. 2 compares the simulated populations of newly-detected planets, for the 6 different scenarios under consideration. Sec. 3.1 discusses some considerations and implications for future years of the Extended Mission, beyond the one-year scenarios that were simulated in detail. Sec. 3.2 discusses the critical issue of the uncertainty in transit ephemerides. Sec. 3.3 discusses the reliability and limitations of our methodology. Sec. 4 concludes and recommends avenues for further study.

Contents

1 Approach	5
1.1 Constraints on possible pointing strategies	5
1.2 Our proposed pointing strategies	5
1.3 Metrics by which we compare pointing strategies	8
1.4 Description of planet detection model	10
1.5 Selecting target stars (and full frame images)	12
1.6 Earth and Moon crossings	17
1.7 Summary of key assumptions and attributes of the planet detection simulations	22
2 Planet detection statistics	25
2.1 Planet yield from the Primary Mission	25
2.2 Planet yield from an example Extended Mission: hemi .	27
2.3 Comparing planet yields from all Extended Missions based on new planet detection metrics	30
2.4 On the brightness of stars with detected planets	39
3 Discussion	39
3.1 Planning Year 3 with Years 4–N in mind	39
3.2 The ephemeris problem	41
3.3 Risks and caveats	45
4 Concluding remarks and recommendations	49
4.1 Recommendations	49
Appendices	52
Appendix A Models relevant to Earth and Moon crossings	52
Appendix B Changes from Sullivan et al. [2015]	55
References	56

1 Approach

1.1 Constraints on possible pointing strategies

The spacecraft has finite fuel reserves for necessary maneuvers, but the reserves are expected to last at least 10 years [G. Ricker, priv. comm.], well past the three-year time horizon that is the focus of this study.

When considering possible schedules for telescope pointings, the main constraint is that the cameras must be directed approximately opposite the Sun. Specifically, the center of the combined fields-of-view is ideally pointed within 15° of the antisolar direction, and no more than 30° away. This is necessary for the sunshade and spacecraft to block solar photons. It also enables the solar panels (which are free to rotate about the $+Y$ axis in Fig. 2) to collect sunlight. Given the spacecraft's orbit [Gangestad et al., 2013], this means that *TESS* should advance $\sim 28^\circ$ east in ecliptic longitude every lunar month, as it does during the Primary Mission. Focusing on a fixed field for say, 3 spacecraft orbits (≈ 42 days), would be in tension with this requirement. In practice, another technical restriction is whether the Earth or Moon passes through *TESS*'s camera fields during a proposed pointing (see Sec. 1.6).

1.2 Our proposed pointing strategies

For simplicity we chose to study one-year plans for an Extended Mission, i.e., plans for Year 3 of the *TESS* mission. (Later in this report we remark on some possible implications of our study for additional

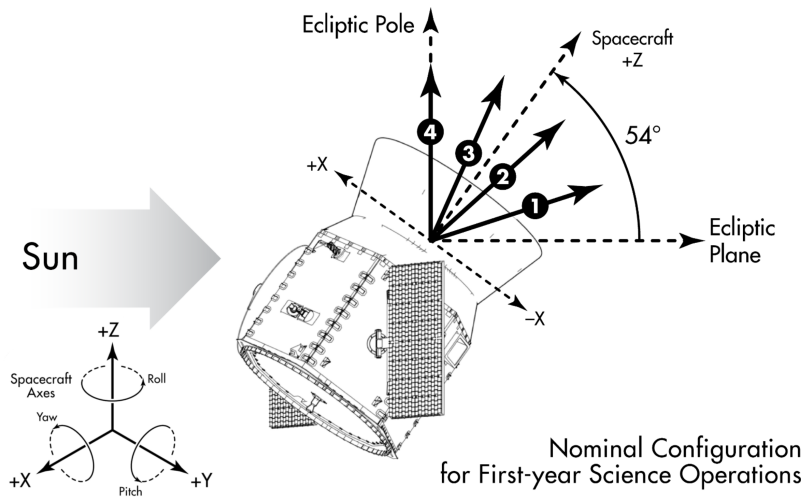


Figure 2: The spacecraft must point so that incident sunlight is collected by the solar panels, and not the cameras. *TESS*'s solar panels pitch about the $+Y$ axis. (Adapted from Orbital ATK design document)

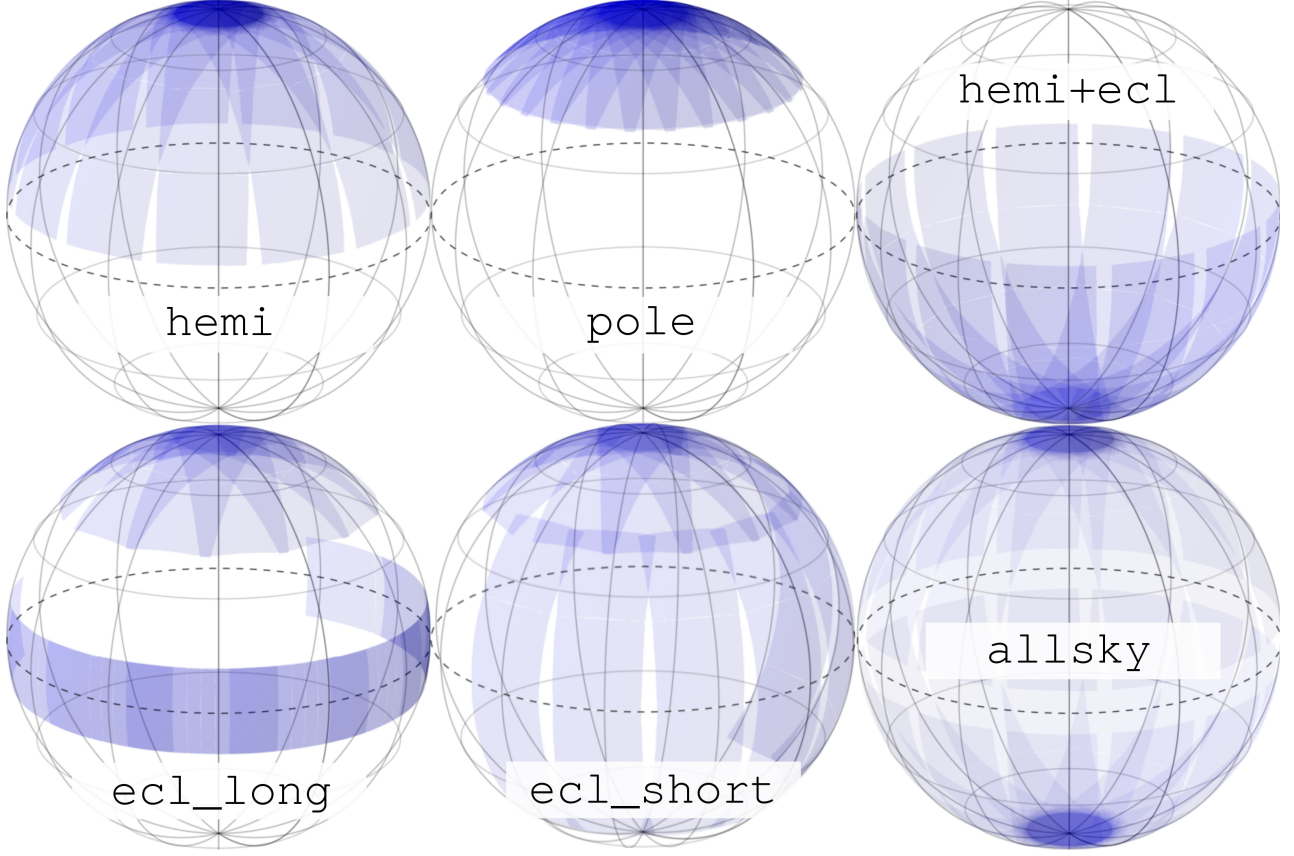


Figure 3: Proposed pointing strategies for a *TESS* Extended Mission, visualized in ecliptic coordinates. *hemi*, *pole*, *hemi+ecl*, *ecl_long*, *ecl_short*, and *allsky*. Note for *ecl_long* and *ecl_short* that Earth and moon crossings likely make an entire year looking at the ecliptic impractical (see Fig. 9).

years of an Extended Mission.) Given the constraints outlined in Sec. 1.1, we selected the following options for detailed study:

Option 1. *hemi*: Repeat observations of one of the two ecliptic hemispheres in a manner similar to the Primary Mission, arbitrarily chosen to be the northern ecliptic hemisphere for concreteness. In this scenario we could take the opportunity to shift the longitudes of all sectors by an amount that would enable *TESS* to cover the gaps that were left during the Primary Mission (the “slits” in the sky coverage between ecliptic latitudes of 6–30°). However for simplicity, we opted to observe the same longitudes as in the Primary Mission. *Justification:* similar motivation as the Primary Mission. Nice long time baseline at the North Ecliptic Pole, and broad sky coverage. Also remeasures transit times (and sharpens ephemerides) of previously detected *TESS* planets over most of the entire hemisphere.

Option 2. *pole*: Focus on one of the ecliptic poles, arbitrarily chosen to be the north ecliptic pole for concreteness. Note that the geom-

etry of *TESS*'s lens hood still suppresses incoming sunlight in this scenario. *Justification:* maximizes the average duration of observations per star; intuitively we expected this to provide greatest sensitivity to long-period planets.

Option 3. hemi+ecl: Repeat observations of one of the two ecliptic hemispheres, but in this case shifting all fields 12° toward the ecliptic, such that the combined fields-of-view reach all the way from 6° below the ecliptic to the ecliptic pole. *Justification:* trades the long continuous viewing zone near the pole for greater sky coverage, and in particular, coverage of the ecliptic zone which was missed in the Primary Mission. We chose to simulate the southern ecliptic hemisphere, since the northern version of this plan would suffer more from Earth and Moon interference (cf. Table 1 in Sec. 1.6).

Option 4. ecl_long: Survey the ecliptic with 7 sectors (14 orbits) in which the long axis of the fields-of-view are oriented along the ecliptic. For the other 6 sectors, during the interval when ecliptic observations would be interrupted by Earth and Moon crossings, we focus on one of the ecliptic poles. *Justification:* covers the ecliptic, which was not surveyed at all in the Primary Mission. Offers opportunities for follow-up of K2 discoveries. Minimizes Earth-moon interference.

Option 5. ecl_short: Survey the ecliptic and also cover a large fraction of the rest of the ecliptic hemisphere. For 7 sectors we observe the ecliptic but with the *short* axis oriented along the ecliptic, and the long axis reaching up to higher latitudes. The remaining 6 sectors are focused on the ecliptic pole, as in *ecl_long*. *Justification:* similar to *ecl_long*, but with more overlap between this year and the Primary Mission to allow for improved transit ephemerides and better ability to follow-up on previous discoveries. Also covers more sky than *ecl_long*, which could improve the quantity of planet detections from full frame images.

Option 6. a11sky: Cover both northern and southern ecliptic hemispheres in a single year, by alternating between the hemispheres every 13.7 days. *Justification:* rapid coverage of the entire sky, allows follow-up of almost all previously detected *TESS* objects and refined ephemerides.

Although these 6 seemed like good options for further study and direct comparison, there are many other possibilities that may be of interest that were not studied in detail, in order to keep the scope of this report manageable. Among these other possibilities that were considered but not studied are

- The pole strategy applied to the south ecliptic pole rather than the north (we do not expect major differences).
- The hemi strategy applied to the southern ecliptic hemisphere rather than the northern (we do not expect major differences). Similarly, the hemi strategy, but rotated about the ecliptic polar axis by 12° in longitude.
- The north/south inversion of hemi+ecl, which is more strongly affected by Earth and Moon crossings (see Sec. 1.6).
- A full year spent observing the ecliptic. Such a plan would similarly suffer from Earth and Moon crossings for a substantial fraction of the year. We show the outage as a function of time in Fig. 9. Solar system objects (planets, asteroids) could also be an annoyance, but we do not model their effects.
- Alternate between northern and southern ecliptic poles every 13.7 days. This would be similar to allsky but would focus on the poles rather than the entire sky. It would sacrifice sky coverage (and ability to refresh ephemerides over the whole sky) in return for longer-duration observations for a typical star.
- Hybrid strategies that change from month to month. For instance, in the hemi scenario, during a month when the Earth or Moon crosses through the field of a camera pointed close to the ecliptic, we could tilt all the cameras away from the ecliptic as in the pole scenario.

1.3 Metrics by which we compare pointing strategies

We assess Extended Missions based on the risks and opportunities they present, as well as through their performance on select technical and science-based criteria. These criteria are organized following an approach originally outlined by Kepner and Tregoe [1965]. Summarizing them in list form:

Technical musts: Cameras anti-sun? Solar panels collecting sunlight?

Technical wants: Duration of each sector < 28 days? Earth or Moon crossings? Zodiacal background? Scattered sunlight off lens hood?

Metrics in exoplanet science:

- number of newly detected planets (from 2-minute cadence fixed-aperture target stars, colloquially ‘postage stamps’, as well as 30-minute full frame images – both independently and combined);

- number of new long-period planets (which may be detected through long period coverage, or by follow-up on single-transit events);
- number of new habitable-zone planets;
- number of new planets with “characterizable” atmospheres;
- number of newly detected planets with bright host stars;
- number of stars with transiting planets detected in the Primary Mission for which the Extended Mission reveals an additional transiting planet (usually long- P companions to short- P transiting planets);
- ability to improve transit ephemerides for previously detected transiting planets;
- ability to observe more transits over a longer baseline to enable searches for transit-timing variations.

These metrics were chosen for their apparent importance as well as our ability to quantify them with simulations. Of course there are other considerations that may be very important but are more difficult to quantify:

- Prospects for altering target allocation weights between: white dwarfs, known planet-hosts, candidate planet-hosts, circumbinary & circumprimary planets, open clusters, evolved stars (notably to detect asteroseismic oscillations), dwarf stars later than M7, stars with well-measured properties,
- Prospects for observations relevant to stellar astrophysics, many of which may overlap with exoplanetary science. For instance, we may wish to try and measure a large sample of stellar rotation periods, or allocate a larger fraction of the data mass for short-cadence asteroseismic targets. We may also wish to observe optical/near-IR variable targets across the sky, in particular pulsating stars (Cepheids, RR Lyrae, Delta Scuti, slowly pulsating B stars), eruptive stars (protostars, giants, eruptive binaries, flare stars), cataclysmic variables (dwarf novae, novae, supernovae), rotating variable stars (deformed by ellipsoidal variations, showing variability from stellar spots or magnetic fields), and eclipsing binaries.
- Prospects for solar-system science, such as observations of main belt asteroids and the brightest near Earth asteroids.
- Prospects for extragalactic astronomy and high energy astrophysics; for instance, gathering light curves of variable active galactic nuclei.

Regarding opportunities and risks, the following need to be considered:

Opportunities:

- What's best on a > 1 year horizon for planet detections? For instance, if it were known in advance that *TESS* would continue operations for several additional years (or even 10 years), would such knowledge affect the optimal choice of the immediate one-year plan?
- Ability to move targets detected in FFIs to PSs in Extended Mission
- Shorten the cadence of FFIs & lengthen the cadence of 'target' stars.
- *TESS as follow-up mission:* ability to observe *CoRoT* objects; ability to observe *Kepler* field (key benefits in broader science wants above); ability to observe *K2* fields (follow-up *K2* few-transit objects); ability to observe targets previously monitored by ground-based surveys.
- *Follow-up for TESS:* potential for *JWST* follow-up? Potential for *CHEOPS* follow-up? Ability to get *TESS* photometry contemporaneously with ground-based observations? Ability to observe from both North and South hemispheres on Earth?
- Impact on Guest Investigator program?

Risks: Risk of spacecraft damage? Risk of not meeting threshold science (to be defined)? Risk of excessive false positives, for instance from crowding? Would partial instrument failure in Primary Mission make this scenario infeasible? Would reduced precision (from aged CCDs, worse pointing accuracy, or other mechanical sources) invalidate this scenario? Risk of planet detection simulation over or under-estimating planet yield?

1.4 Description of planet detection model

Sullivan et al. [2015] (hereafter, S+15) developed a simulation of *TESS*'s planet and false positive detections based on the spacecraft and payload design specified by Ricker et al. [2014]. We adapt this simulation for Extended Mission planning. With our additions, we can change where *TESS* looks in additional years of observing while holding fixed all other mission-defining parameters. Our approach is then to run our planet detection simulation for each plausible pointing strategy, and to compare the relative yields of detected planets. This lets us compare Extended Mission scenarios with one another and with the Primary Mission.

Background on synthetic catalogs: *TESS* is sensitive to sub-Neptune sized transiting planets orbiting M dwarfs out to $\lesssim 200$ pc and G dwarfs out to $\lesssim 1$ kpc (S+15, Sec. 2.3). It is sensitive to giant planets and eclipsing binaries across a significant fraction of the galactic disk. With this sensitivity in mind, the stellar catalog we ‘observe’ in our planet detection simulation is drawn from the output of TRILEGAL, a population synthesis code for the Milky Way [Girardi et al., 2005]. S+15 made some modifications to the catalog, notably in the M dwarf radius-luminosity relation, to better approximate interferometric stellar radii measurements. We retain these modifications; the modified TRILEGAL stellar catalog shows acceptable agreement with observations², specifically the Hipparcos sample [Perryman et al., 1997, van Leeuwen and Leeuwen, 2007] and the 10pc RECONS sample [Henry et al., 2006].

With a stellar catalog defined, we populate the stars in the catalog with planets based on occurrence rates derived from the *Kepler* sample. We use rates Fressin et al. [2013] found for planets orbiting stars with $T_{\text{eff}} > 4000$ K and those that Dressing and Charbonneau [2015] found for the remaining M and late K dwarfs.

Detection process: We then simulate transits of these planets. Assuming the transit depth and number of transits are known, we use a model of *TESS*’s point spread function (PSF) to determine optimal photometric aperture sizes for each postage stamp star (*i.e.*, we compute the noise for all plausible aperture sizes, and find the number of pixels that minimizes this noise). With the aperture sizes and noise corresponding to a given integration time known, we compute a signal to noise ratio for each transiting object. Our model for planet detectability is a simple step function in SNR: if we have two or more transits and $\text{SNR} > 7.3$, the planet is ‘detected’, otherwise it is not³. Our model for *TESS*’s photometric precision is described by S+15 and shown in Fig. 7.

Assumptions of SNR calculation: Our approach to computing SNRs for each transiting object is not time-resolved. In other words, we are not simulating every 2 second CCD readout, stacking those hypothetical readouts into 2 minute cadence postage stamps and 30 minute full frames, and then reducing simulated light curves.

Our calculation is simpler. We assume perfect period-recovery, phase folding, and identical conditions between transits. We also assume that we observe a constant transit depth, which is diluted by binary companions and background stars in the same manner between transits. Our approach is then to simply tally the number of *TESS* fields a given host star falls within, which corresponds to a

² Looking closely at the radius-luminosity relations, we do see non-physical interpolation artifacts. These outliers are visible in Figs. 5 and 6 below, but are a small enough subset of the population that we ignore them for this work.

³ The value of this threshold is chosen to ensure that no more than 1 statistical false positive is present in a pipeline search of 2×10^5 target stars. Observing a greater number of stars, for instance in full frame images, should require a higher threshold value to maintain the same condition. We discuss this further in Sec. 3.3.

known total observing baseline. Assuming random orbital phasing, we then compute the number of transits *TESS* observes for planets of any given host.

With a model PSF, we determine ideal aperture sizes and then obtain an accurate noise per transit (since the transit durations are known, and we assume our noise, computed first over a single hour, then bins like white-noise, *i.e.*, proportional to the inverse square root of the time in-transit).

Coupled with the known transit signal, this gives us the SNR per transit, and then to ‘phase-fold our light-curves’ (light-curves which are never explicitly computed point-by-point) we just⁴ multiply the SNR per transit by the square root of the number of transits observed.

Summarizing the relevant terms in an equation,

$$\begin{aligned} \text{SNR}_{\text{phase-folded}} &\approx \sqrt{N_{\text{tra}}} \times \text{SNR}_{\text{per-transit}} \\ \text{SNR}_{\text{phase-folded}} &= \sqrt{N_{\text{tra}}} \times \frac{\delta \cdot D}{\left(\frac{\sigma_{\text{1hr}}^2}{T_{\text{dur}}} + \sigma_v^2 \right)^{1/2}}, \end{aligned} \quad (1)$$

for δ the undiluted transit depth; D the dilution factor computed from background and binary contamination (Eq. 3); σ_{1hr} the summed noise contribution from CCD read noise, photon-counting noise from the star, a systematic $60 \text{ ppm} \cdot \text{hr}^{1/2}$ noise floor, and zodiacal noise; T_{dur} the transit duration in hours, and σ_v the intrinsic stellar variability (cf. S+15 Sec 3.5). The first equation is approximate. In particular we do not take into account the small contribution to the SNR from occultation signals.

We have changed other aspects of this simulation since S+15 was published, and describe these changes in Sec. B of the appendix.

1.5 Selecting target stars (and full frame images)

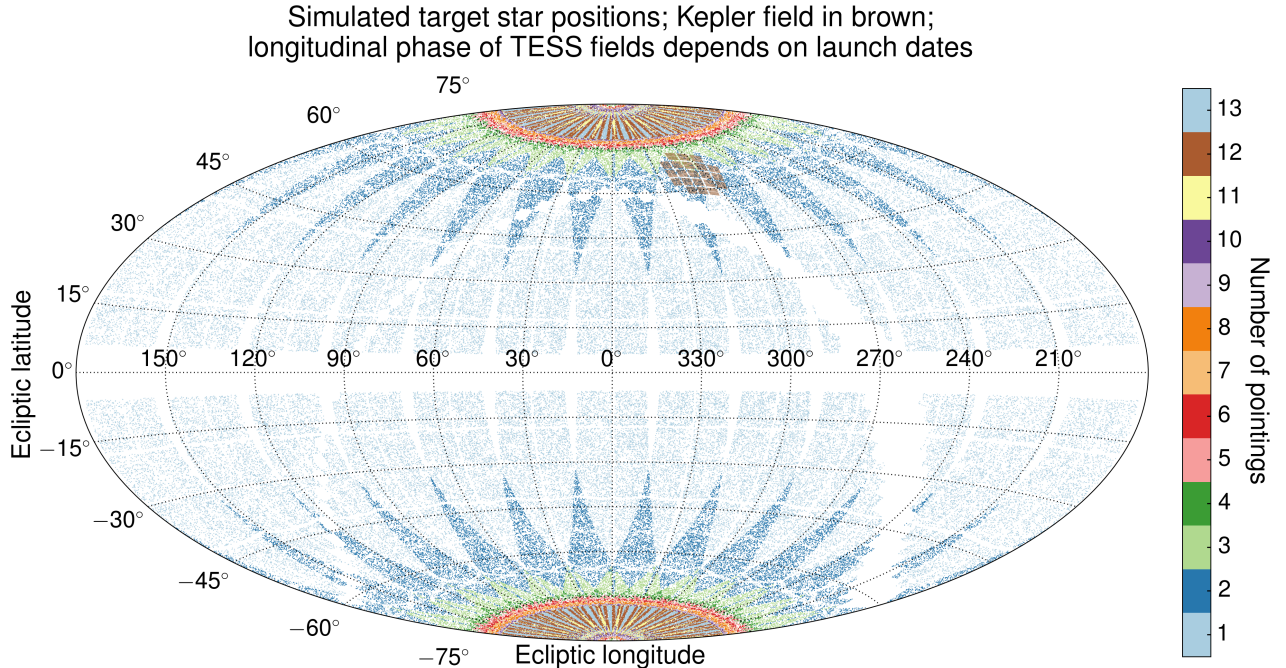
For the Primary Mission, *TESS*’s short cadence (2 min) targets will be drawn from a subset of the *TESS* Input Catalog. The prioritization statistic that the mission will use in this selection has yet to be explicitly defined.

We know that for *TESS* to detect small transiting planets it should observe stars that are small and bright. For this work, we define a simple statistic, **Merit**, proportional to the SNR we should expect from an arbitrarily sized planet orbiting any star:

$$\text{Merit} \equiv \frac{1/R_*^2}{\sigma_{\text{1-hr}}(I_c)/\sqrt{N_{\text{obs}}}}, \quad (2)$$

where R_* is the radius of the star in question, $\sigma_{\text{1-hr}}$ is the relative precision in flux measurements over one hour of integration time, taken

⁴ We actually take a quadrature sum of both transit and occultation signals, but this is negligible for planets. It only matters for the case of eclipsing binaries, which we ignore in this work.



from an empirical fit to Fig 7, I_c is the Cousins band I magnitude TESS observes for the star (or more precisely, the star system) and N_{obs} is the number of observations the star receives over the course of the mission. For multiple star systems, R_\star is taken to be the radius of the planet-hosting star, and the I_c magnitude is based on the combined flux from all the stars.

We evaluate Merit for all the star systems in our modified TRILEGAL catalog, and then choose the best 2×10^5 as target stars to be observed at 2 minute cadence. Target stars selected in this manner are shown in Fig. 4. This statistic is simpler than the procedure outlined in Section 6.7 of S+15 and it produces a nearly identical population of target stars (shown in Fig 5). Our approach for full frame image simulation is different from that of S+15, and we describe it below.

We generalize our Merit statistic to Extended Missions as follows: over an entire mission, the total number of observations a star receives is the sum of its observations in the Primary and Extended Missions: $N_{\text{obs}} = N_{\text{primary}} + N_{\text{extended}}$. If $N_{\text{extended}} = 0$ for a given star, then do not select that star as a target star in the Extended Mission. Else, compute its Merit (Eq. 2) weighted by $N_{\text{obs}} = N_{\text{primary}} + N_{\text{extended}}$. In this manner stars that are observed more during the Primary Mission are more likely to be selected dur-

Figure 4: Selected target stars in the Primary Mission. Their density increases towards the poles because of the $\sqrt{N_{\text{obs}}}$ weight in selection. Dead space on the CCDs creates ‘gaps’ in the continuous viewing zones.

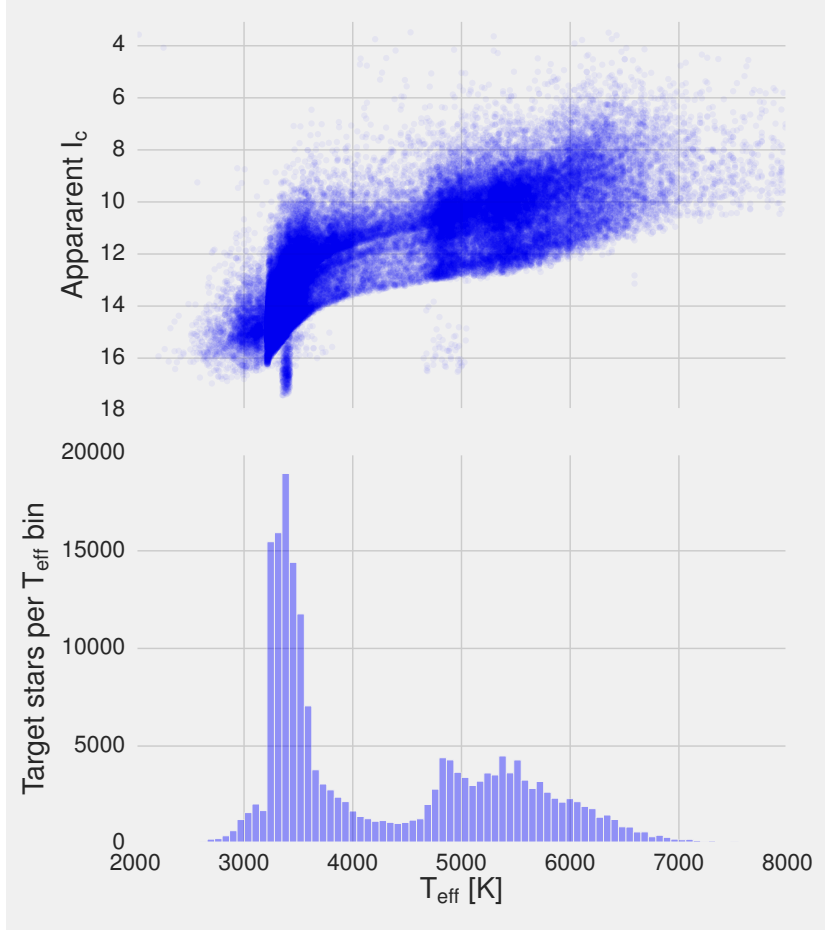


Figure 5: Target star Cousins I magnitude against effective temperature (replicates Figure 17 of S+15). Target stars are selected as the best 2×10^5 stars according to $\text{Merit} \equiv \sqrt{N_{\text{obs}}(1/R_*^2)/\sigma_{1\text{-hr}}(I_c)}$. The top subplot shows 1 in 10 stars. This simple model could inform the target selection to be performed on the TESS Input Catalog. The lower histogram is bimodal, selecting heavily for M dwarfs, and selecting more F and G dwarfs than K dwarfs. This shape arises from the combined $1/R_*^2$ and $1/\sigma_{1\text{-hr}}(I_c)$ weights: the fact that the minimum falls around K dwarfs occurs because of both a Malmquist bias (there are more F than K stars of comparable brightness in our catalog from which to select) as well as a corresponding dip in the TRILEGAL (& observed) V -band luminosity functions (see S+15 Figure 5).

Outliers visible in the upper scatterplot are non-physical, possibly artifacts from S+15’s Padova-to-Dartmouth interpolation as they tend to have greater masses than all other stars on the main sequence. As they comprise less than 1% of the target stars, we ignore them in order to proceed.

ing the Extended Mission.

Alternative prioritization approaches: It is worth emphasizing that our scheme for selecting target stars for an Extended Mission does not make use of any information on whether candidate transit events were observed during the Primary Mission. If a star were observed at short cadence for an entire year, and no candidate events were found, it might be sensible to disregard that star in the Extended Mission in favor of stars that have never been observed at short cadence – particularly those with candidate events that were detected in the Primary Mission full-frame images. These and related concerns are discussed further at the accompanying Wiki document⁵.

More abstractly, the procedure of simply applying Eq. 2 attempts to select a stellar sample that will yield the most small transiting planets around the brightest stars. An alternative approach would be to select stars that will give the most *relative benefit* in 2 minute

⁵ <https://facebook.mit.edu/display/TESS/Extended+Missions>

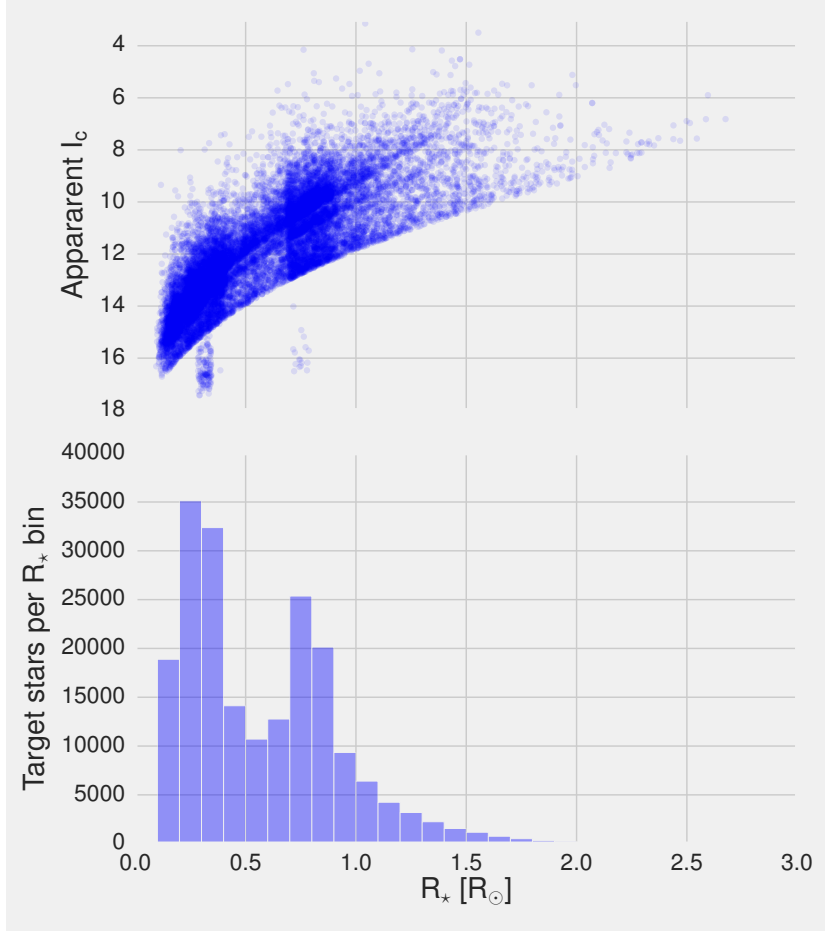


Figure 6: Same as Fig. 5, but as a function of stellar radius. $1/R_*^2$ selection weight clearly visible, along with the same outliers.

postage stamps over 30 minute cadence observations since all stars will be present in the 30 minute images. This ‘relative benefit’ could be a function of improved transit detectability, or perhaps improved capacity to resolve the partial transit phases.

For purposes of transit detection, the difference between 2 and 30 minute cadence matters most when transits have short durations – in other words for small stars, and for close-in planets. Switching to this alternative approach would consequently bias us even more strongly towards selecting M dwarfs. We already select almost every M dwarf with $I_c < 14$. The limiting I_c magnitude for detecting $R_p > 4R_\oplus$ planets with *TESS* is ~ 16 , which is where we see the dimmest stars in Fig. 5.

Additionally, the procedure of applying Eq. 2 and assuming that it will maximize the number of small planets that *TESS* will detect about bright stars ignores the functional dependence of planet occurrence rates on stellar properties. For instance, should we prioritize

target stars that are metal-rich? Metal-rich stars demonstrably host more giant planets within *TESS*'s period sensitivity than metal-poor stars [Fischer and Valenti, 2005, Johnson et al., 2010]. The question of whether this correlation extends to sub-Neptune radius planets is somewhat contested, but for instance Wang and Fischer [2015] used a sample of KOIs and found that the planet occurrence rates of (gas dwarf) planets are $1.72^{+0.19}_{-0.17}$ ($2.03^{+0.29}_{-0.26}$) higher around metal-rich than metal-poor stars. Note that in this study, ‘terrestrial’ means $R_p < 1.7R_{\oplus}$, ‘gas dwarf’ $1.7R_{\oplus} < R_p < 3.9R_{\oplus}$, and the authors focused only on solar-type stars ($4800 \text{ K} < T_{\text{eff}} < 6500 \text{ K}$).

A more robust approach for *TESS*'s target selection might take these kinds of results into account probabilistically. For instance, Kipping and Lam [2016] note that the probability of short-period transits having additional transiting outer companions is functionally dependent upon the properties of the short period transits – for instance their orbital periods and radii. They navigate the optimization problem using artificial neural networks (ANNs) trained to select for features that improve the probability of detecting transiting outer companions. *TESS* might benefit from a similar approach in target selection.

Alternative prioritization approaches in Extended Missions: Our Merit statistic also neglects the option of an Extended Mission which only observes stars with known planets or planet candidates (*TESS*'s objects of interest, or those from other transit and RV surveys) at short cadence. This approach would free up a considerable portion of *TESS*'s data mass for full frame images at e.g., 15 minutes rather than the current nominal 30 minutes.

Approach to full-frame images: We want to simulate the full frame image detections in a computationally tractable manner. While S+15 evaluated the phase-folded SNR for every potentially transiting object about each of the $\sim 1.6 \times 10^8$ stars in our synthetic catalog, we focus only on the stars for which *TESS* could plausibly detect a sub-Neptune planet over the 3-year mission. Most stars that *TESS* sees are too dim or too large to detect $R_p < 4R_{\oplus}$ planets – while we expect many giant planet detections towards the galactic plane (S+15 Fig 19), small-planet detections are more nearly isotropic, since practically all occur for stars at $< 1 \text{ kpc}$. For our purposes in this study, we argue that knowing there will be thousands of giant planet candidates is sufficiently accurate. The prospects for detecting smaller planets are more likely to help discriminate between different scenarios for the Extended Mission.

In this vein, we only simulate full frame image detections for the

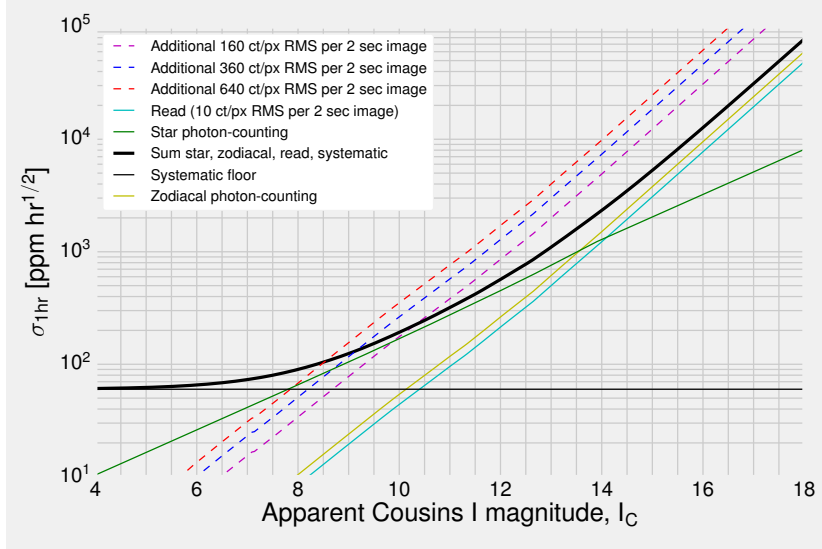


Figure 7: Relative precision in measured flux over a one hour integration time (scatter from contaminating background stars and PRF centroid offsets ignored). The noise sources described by Sullivan et al. [2015] are solid thin lines. The dashed lines exemplify noise from contaminating background flux, for instance from the Moon or Earth outside the *TESS* field, but still scattering light off the *TESS* lens hood. A dynamical 3-body simulation lets us estimate the impact lunar and Earth backgrounds have on *TESS*'s photometry. The photometric precision with which we simulate observations has additional scatter about the thick black line owing to randomly-assigned contaminating stars. Zodiacal background is plotted for an ecliptic latitude of 30° following Sec. 6.4.1 of Sullivan et al. [2015]

3.8×10^6 highest Merit stars following the 2×10^5 highest Merit stars observed as ‘postage stamps’. This number (3.8×10^6) was initially estimated based on the number of searchable stars about which we expect *TESS* to be able to detect sub-Neptune radius planets [Winn, 2013b]. The detection process is then identical to that for postage stamps, except with 30 minute instead of 2 minute exposures, which increases the apparent durations and shrinks the apparent depths for transits with durations of $\lesssim 1$ hour. To ensure that 3.8×10^6 stars is sufficient to include all stars about which *TESS* might detect sub-Neptune radius planets, we repeated this process for the Primary Mission using 5.8×10^6 , 9.8×10^6 and 19.8×10^6 ‘full frame image’ stars, and confirmed that there was no significant difference in the planet yields at $R_p \leq 4R_\oplus$ between any of the cases. Increasing the number of FFI stars, the runs yield increasing numbers of giant planets, particularly near the galactic disk. Meanwhile the number of sub-Neptune radius planets remains fixed, and thus convinces us that our simulation includes a sufficient number of target stars to be complete for sub-Neptune detection statistics.

1.6 Earth and Moon crossings

When the Earth or Moon passes through *TESS*'s camera fields they can flood the CCD pixels to their full well capacity ($\sim 2 \times 10^5$ photoelectrons). Precision differential photometry becomes impossible in any pixels that are directly hit during these crossings. Even when the body (Earth or Moon) is not directly in the camera's field of view, its light scatters off the interior of spacecraft's lens hood and acts as

a background source of contaminating flux across many of the cameras⁶. The Poisson noise in the number of photons arriving from the Earth or the Moon in such a scenario degrades *TESS*'s photometric performance.

We show a few example background fluxes in Fig. 7. The point of this figure (aside from showing *TESS*'s baseline noise budget) is that additional scattered light could reduce *TESS*'s photometric performance. For instance when the Moon is 24° from the camera boresights the lens hood is expected to suppress $1/100^{\text{th}}$ of a mean $3 \times 10^6 \text{ ct}/\text{px}$ (per 2 second image) from incoming moonlight⁷. Thus a mean flux of $3 \times 10^4 \text{ ct}/\text{px}$ reaches the cameras. The RMS is then roughly $173 \text{ ct}/\text{px}$ per 2 second image. From Fig. 7, this corresponds to $\gtrsim 3 \times$ worse photometric performance for stars with $I_c < 12$. While this effect is highly dependent on the angle between the camera boresights and the Moon or Earth, the general picture is that for field angles $\theta \lesssim 25^\circ$, the impact can be severe.

Separately from our planet detection simulation, we study these crossings in a dynamical simulation based on JPL NAIF's standard SPICE toolkit. Given a nominal launch date, this code determines *TESS*'s orbital phasing throughout its entire mission. At every time step of the three-body orbit, we calculate the distance between *TESS* and the other two bodies of interest, and the separation angles among each of the four cameras and each of the two bodies (eight angles in total). The gravitational dynamics behind this calculation treat the Earth, Moon, and Sun as point masses, and the *TESS* spacecraft as a massless test particle. The spacecraft's inclination oscillates in the simulation as it will in reality.

Taking the Earth and Moon's integrated disk brightnesses as fixed values⁸ we use a model for scattered light suppression from the *TESS* lens hoods (Fig. 25) to compute the mean photon flux from each of these bodies onto each of the cameras throughout the orbit. We then compute the corresponding variance in incoming flux, and compare it to *TESS*'s noise budget.

To evaluate the cumulative impact of Earth and Moon crossings on *TESS*'s Primary and Extended Missions we ask: for each camera, what fraction of the total observing time is *TESS* unable to operate at desired photometric precision because of Earth and Moon crossings? An upper limit for what we mean by 'unable to operate at desired photometric precision' is when terrestrial or lunar flux make it impossible to observe a sizable portion of the stars in the *TESS* target star catalog with reasonable precision. For example, Fig. 26 shows that $\sim 80\%$ of the stars that could be observed at sub-mmag precision over an hour no longer can when the Earth is 17° from the camera boresight. This of course depends on the target star catalog's ap-

⁶ A detailed model for this process is not yet available.

⁷ Our model for suppression as a function of angle is appended in Fig. 25

⁸ The full moon's apparent magnitude is $I_M \approx -13.5$. Scaling from photon fluxes tabulated in Winn [2013a], this gives $2.5 \times 10^{13} \text{ ct/s}$. Averaging over the focal plane array, this means a mean additional flux per image of $3 \times 10^6 \text{ ct}/\text{px}$. The relevant variance is (roughly) the square root, $\approx 1730 \text{ ct}/\text{px}$ per 2 sec image. The Earth is roughly $80 \times$ brighter, giving mean additional flux per image of $2.4 \times 10^8 \text{ ct}/\text{px}$, or an RMS of $\approx 15500 \text{ ct}/\text{px}$ per 2 sec image. This substantiates the claim that the Earth and Moon flood the cameras to their full well capacity. The effect on observing precision is appended in Fig. 26.

	Camera 1	Camera 2	Camera 3	Camera 4
Year 3 selected				
pole	0	0	0	0
hemi	2	1	0	0
hemi+ecl	2	0	0	0
ecl_long	1	1	1	1
ecl_short	0	1	1	0
allsky	1	1	0	0
Year 3 omitted				
pole (south)	0	0	0	0
hemi (south)	1	0	0	0
hemi+ecl (south)	4	3	0	0
ecl_long (1yr)	4	4	4	4
ecl_short (1yr)	1	3	4	2
allsky (poles)	0	0	0	0
Primary Mission				
hemi (south year 1)	2	1	0	0
hemi (north year 2)	4	2	0	0

Table 1: Number of sectors (of 13 per year) ‘dropped’ due to the Earth and Moon crossings in both selected and omitted Extended Missions, with those of the Primary Mission for reference. The method of ‘dropping’ fields (which neglects the temporal nature of the crossings, discussed in the text) gives a representative sense of the cumulative impact of Earth and Moon crossings. Scenarios with (south) appended refer to their counterparts in the southern ecliptic hemisphere. `ecl_long (1yr)` corresponds to a full year with the *TESS* field’s long axis along the ecliptic, and `ecl_short (1yr)` corresponds to the same, but with the short axis along to the ecliptic. These scenarios are neglected because their outages are time-correlated (see Fig. 9). `allsky (poles)` would be a scenario that observes in the manner of `allsky`, but only on the ecliptic poles as in `pole`.

parent magnitude distribution (Fig. 5), and the cutoff of ‘sub-mmag precision over an hour’ is somewhat arbitrary.

Developing a detailed model of how these crossings impact *TESS*’s photometry is beyond the scope of this work. To account at least qualitatively for their effect in our simulation we adopt a simple approximation: we impose that a camera has an ‘outage’ if there are over $F_{\text{thresh}} \equiv 300 \text{ cts}/\text{px/s}$ (an additional RMS of $\approx 25 \text{ ct}/\text{px}$ per 2 sec image). We then compute the time-averaged fraction of each observing sector for which *TESS*’s cameras remain above this threshold. A given sector has ~ 660 hours of observing time over two spacecraft orbits. As an example, suppose that 220 of these hours had the Earth, the Moon, or both shining with a background flux $F > F_{\text{thresh}}$. This would correspond to a fractional outage of $1/3$. We then compute the mean of this fractional outage across all 13 annual sectors to derive a ‘mean camera outage’ for each proposed pointing scenario. We then approximate the effect of Earth and Moon crossings by selectively omitting the closest integer number of observing sectors corresponding to the ‘mean camera outage’ described above. For instance, if the ‘mean camera outage’ was 17% of *TESS*’s observing time over a given year, we would omit the 2 (of 13) observing sectors that suffer the greatest number of lost hours, for that given camera. The relevant number of omitted sectors is shown in Table 1; an example of the resulting spatial distribution of detected planets is shown in Fig. 11.

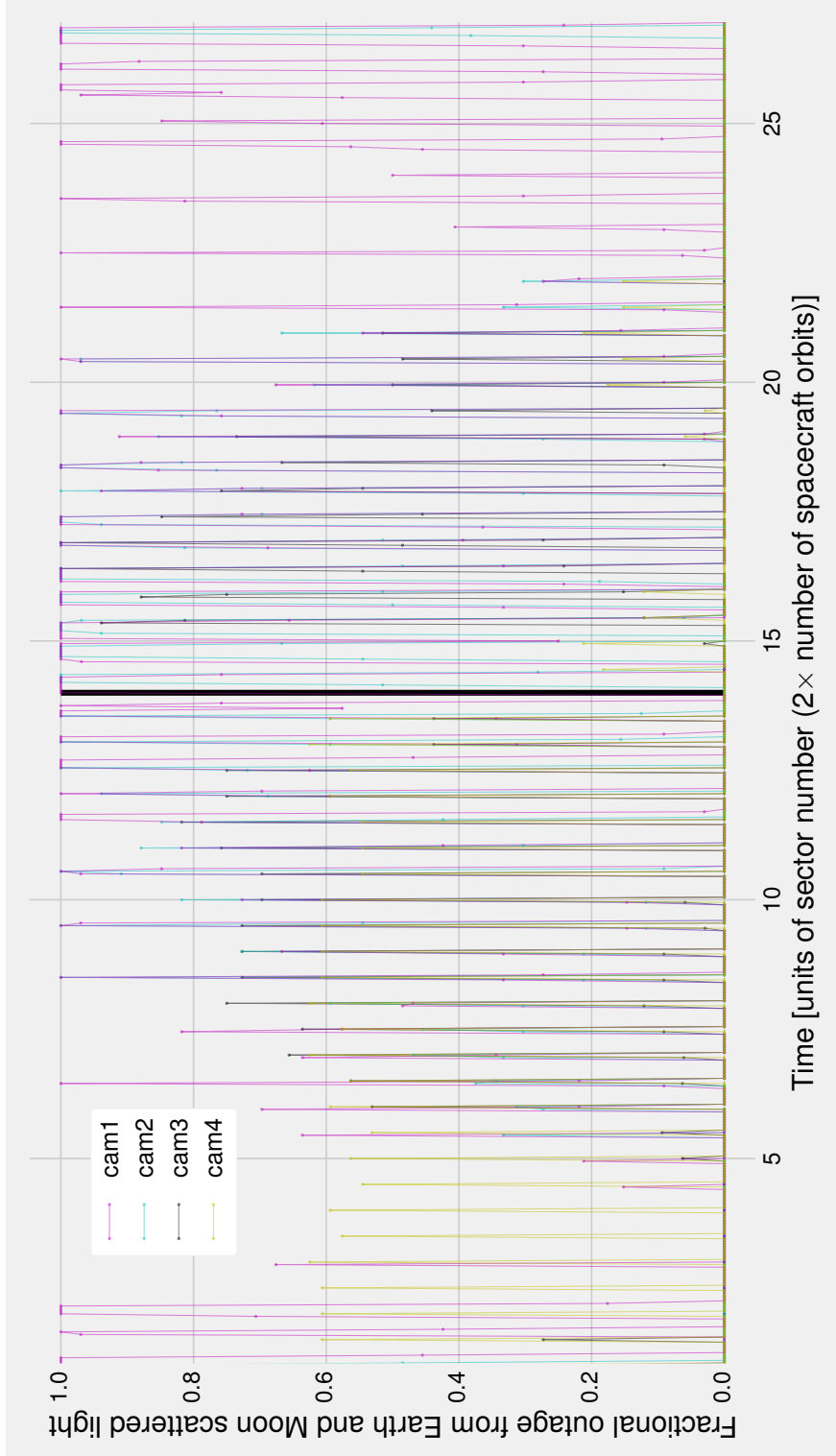


Figure 8: ‘Outage’ caused by Earth and Moon crossings as a function of time in the orbit. Specifically, the y -axis shows the probability of having a polluted frame with mean incident earthlight or moonlight of $> 300 \text{ ct}/\text{px}/\text{s}$ in a time-step bin of $1/20^{\text{th}}$ of an orbit (where the probability is the number of polluted frames divided by the total number of frames in that bin). The mean of this outage across any given year is used to compute the number of dropped fields in Table 1, which should then be an upper bound to the impact of Earth and Moon crossings. In this plot, the first year of observations are in the southern ecliptic hemisphere. The black dividing line indicates the beginning of ‘Year 2’ (northern hemisphere). The worst fractional outage per orbit is in Camera 1, which points towards the ecliptic, over the first ~ 5 orbits of the second year. The plot has ‘spikes’ because outage typically only occurs over a small fraction of the orbit.

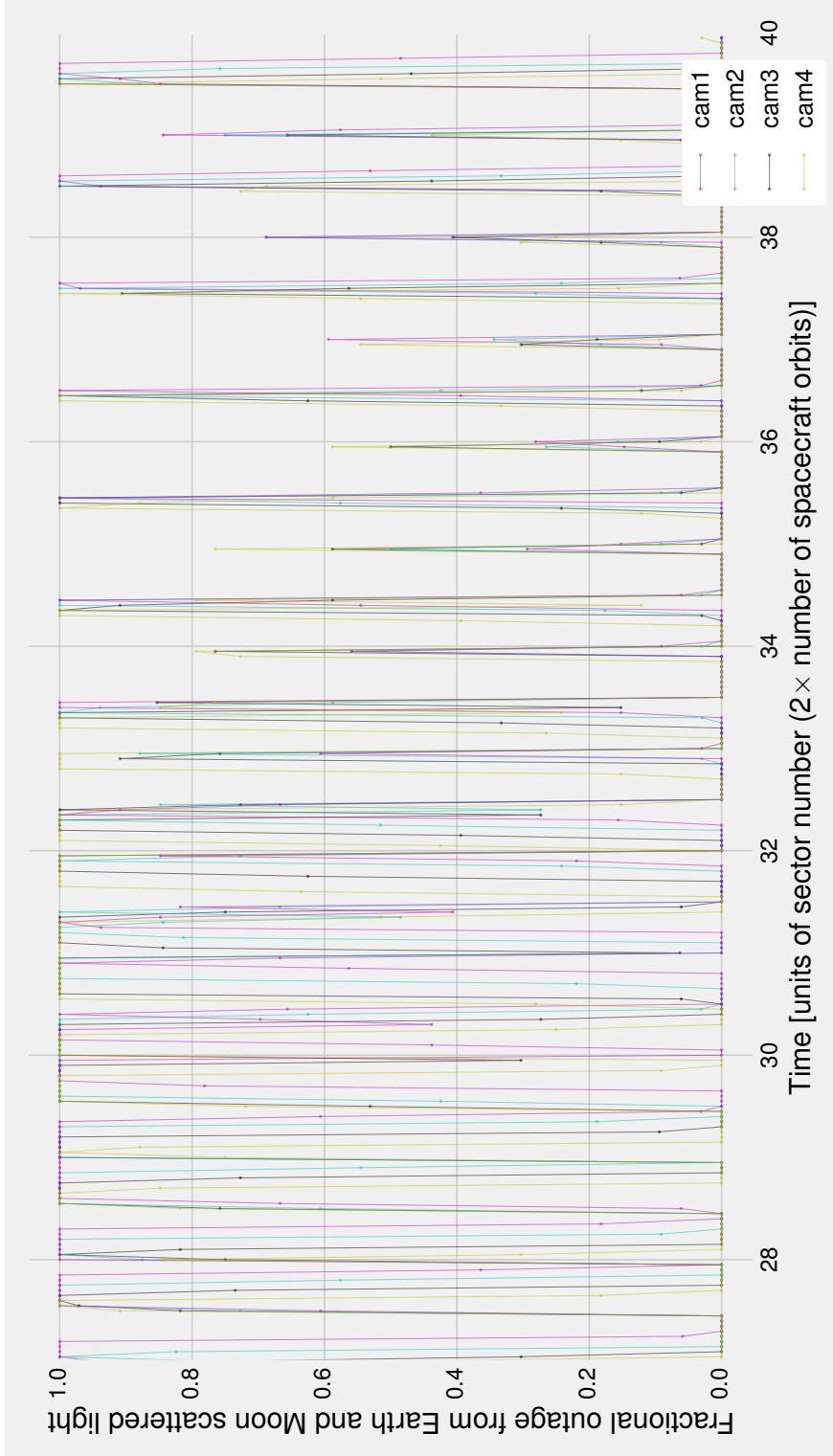


Figure 9: Same as Fig. 8, except for a hypothetical third year in which TESS observes the ecliptic with the cameras’ long axis along the ecliptic plane for the entire year. The latter half of the year experiences far less Earth and Moon interference than the first half. Considering it implausible that we would opt to sacrifice such a large fraction of our observing time, we study the `ecl_long` and `ecl_short` scenarios instead, as their observations avoid this effect during the first ~ 5 months.

As mentioned in Sec. 1.4, our planet detection simulation is not explicitly time-resolved; it uses the ecliptic coordinates of camera fields for each orbit as input to compute the observed baselines for each star in our galactic model. While our Earth/Moon crossing procedure ignores the temporal nature of the ‘outages’ (which is shown resolved over time-steps of $1/20^{\text{th}}$ of an orbit in Figs. 8 and 9), it gives a conservative sense of the cumulative impact of Earth and Moon crossings over the course of a year.

Our approximation is ‘conservative’ in the sense that the additional background corresponding to $F_{\text{thresh}} = 300 \text{ ct}/\text{px}/\text{s}$ only becomes a noticeable noise source for targets later than Mo at $I_c \lesssim 14$ (see appended Fig. 27). This corresponds to a relatively small fraction of the input catalog (18%), being observed with $\lesssim 1.5 \times$ worse RMS precision. By counting all the relevant time as an ‘outage’ lost across all stars (even the bright ones for which the additional scatter is subsumed by shot-noise), we are likely being more sensitive to scattered Earth and Moonlight than *TESS* will be.

The impact of this approximation on the planet yield of the Primary and Extended Missions are discussed in Secs. 2.1 and 2.3 respectively. The summarized result is that this model of Earth and Moon crossings leads to $\lesssim 10\%$ fewer $R_p < 4R_{\oplus}$ planet detections compared to the case of not accounting for the crossings at all. There is thus little reason to raise our low threshold, given that the magnitude of the effect is this small. Moreover, the Earth and Moon crossings typically last for a small fraction of an orbit (Fig. 8). If the timescales required for the cameras to ‘re-settle’ after the crossings are small compared to orbital timescales, our approach may overestimate the effect’s importance even further. More detailed models of this process will be developed during the spacecraft’s commissioning period.

1.7 Summary of key assumptions and attributes of the planet detection simulations

- We focus almost exclusively on planets with $R_p < 4R_{\oplus}$.
- We assume the TRILEGAL catalog (modified to match interferometric radii, as described by S+15) is an accurate representation of the stellar neighborhood to $\lesssim 2\text{kpc}$.
- We omit the 5% of the sky closest to the galactic disk (see Fig. 4). We expect that *TESS*’s large pixel size ($21 \times 21''$) combined with crowding near the galactic disk will cause substantial source confusion and a large astrophysical false positive rate in this area. On a practical note, TRILEGAL cannot be queried within its run-time

limit for some of these fields (cf. S+15 Sec 3.1).

- We assume prior knowledge of the radii and apparent magnitudes of TRILEGAL’s synthetic stars, so we can prescribe a simple prioritization statistic (Eq. 2) that we expect (but have not verified) maximizes the number of small planets we discover about bright stars⁹.
- In evaluating a star’s Merit (Eq. 2), we assume an observed magnitude for each star that comes from the sum of the flux from the star itself in addition to any companion and background stars (whose presence will not be known by the mission *a priori*, but which we then account for when computing ‘observed’ SNRs).
- We use occurrence rates of planets as a function of radius and orbital period as calculated by Fressin et al. [2013] and Dressing and Charbonneau [2015]. We assume these are accurate for the $P \lesssim 180$ day planets to which *TESS* is sensitive.
- The occurrence statistics of multiple-planet systems can approximated as repeated independent draws from the single-planet distributions. The orbits of planets in multiple planet systems are coplanar and stable (with period ratios of at least 1.2 between adjacent planetary orbits).
- For our instrument and noise models, we assume:
 - A point-spread function (PSF) derived from ray-tracing simulations, slightly degraded from that described by S+15 Sec 6.1, and based on laboratory measurements.
 - All stars are observed at the *center* of the *TESS* CCDs. This ignores off-axis and chromatic aberrations within the *TESS* optics, and consequently ignores the angular dependence of the pixel response function (the fraction of light from a star that is collected by a given pixel). While S+15 attempted to model the field-angle dependence, we argue that the methodology used in that work was inconsistent (see appendix Sec. B), and that rectifying this approach would be complex and time-consuming. Ignoring the field-angle dependence is a simplification that may lead to loss of accuracy, but since this applies to all the scenarios under consideration, it should still be possible to *compare* the results of different scenarios without much loss of accuracy.
 - The time/frequency structure of all noise (except for stellar variability, see Eq. 1) is ‘white’. This means that we ignore time-correlated instrumental effects such as spacecraft jitter, thermal fluctuations, and mechanical flexure, which we expect will be at least partly mitigated by the mission’s data reduction pipeline.

⁹ Although it is difficult to determine accurate photometric radii, we expect that by the time *TESS* launches *Gaia* will provide parallaxes and proper motions for many *TESS* targets, allowing *TESS* to discriminate between red dwarfs and red giants for purposes of target prioritization.

- We assume the instruments work equally well in year 3 as in years 1 and 2.
- The assumed contributors to white noise include: CCD read noise, shot noise from stars, a systematic noise floor of $60 \text{ ppm} \cdot \text{hr}^{1/2}$, and zodiacal background. See Fig. 7 for the relative contributions of these terms as a function of apparent magnitude.
- The noise contributions from stellar intrinsic variability are assumed to be identical to those described by S+15 Sec3.5, which uses variability statistics from the *Kepler* data computed by Basri et al. [2013]. Unlike all previously mentioned noise sources, we do not scale noise from stellar variability as $t_{\text{obs}}^{-1/2}$, since the photon flux from stars may vary over time-scales similar to typical transit durations. Instead, we assume the noise contribution from stellar variability is independent across transits, and thus scales as $N_{\text{tra}}^{-1/2}$, for N_{tra} the number of observed transits.
- For our detection model, we assume:
 - A step-function detection threshold: for $\text{SNR} \geq 7.3$, we rule transiting planets as detected, for $\text{SNR} < 7.3$, they are not detected.
 - The top 2×10^5 merit-ranked targets (Eq. 2) are observed at two-minute cadence, and the next 3.8×10^6 stars are observed at thirty-minute cadence. We use S+15 Sec. 6.8 approach to ‘blurring’ transits with durations $\lesssim 1\text{hr}$, so that for longer cadence images shorter transits get shallower depths and longer apparent durations. As described in Sec. 1.5, we verify that under this assumption, our detections are complete for $R_p < 4R_{\oplus}$, and incomplete for Jupiter-sized planets.
 - We require ≥ 2 transits for detection. We assume the period can be recovered without ambiguity and likewise there is no ambiguity in identifying which target star is exhibiting a given transit signal.
- We do not assume any prior knowledge of previous observations that may have been performed on our stars. For instance, observing the ecliptic, we do not simulate the *TESS*-K2 overlap.
- For Earth and Moon crossings, we assume we can drop a fixed number of orbits of observing time for the cameras that suffer most from the Earth, the Moon, or both being in *TESS*’s camera fields. We summarize this effect in Table 1. Although this ignores the time-correlated nature of the outages shown in Figs. 8 and 9, it is sufficient for comparing detected planet yields across missions,

and leads to $\lesssim 10\%$ fewer $R_p < 4R_{\oplus}$ planet detections compared to the case of not accounting for the crossings at all.

- We assume that we can (eventually) discriminate between astrophysical false positives (for instance background eclipsing binaries or hierarchical eclipsing binaries) and planet candidates.
- We can compute SNR with effective signal $\delta_{\text{eff}} = \delta \times D$ for $\delta = (R_p/R_{\star})^2$ the transit depth, and

$$D = \frac{\Gamma_N + \Gamma_T}{\Gamma_T} \quad (3)$$

where D is the dilution factor of a target star with incident photon flux Γ_T from the target star and incident photon flux Γ_N from neighboring stars (*i.e.*, background stars or binary companions).

The noise is computed by creating a synthetic image for every host star with a planet that transits above a ‘pre-dilution’ SNR threshold (this threshold is imposed for the sake of lowering our computational cost). This 16×16 pixel image is of the number of photoelectrons *TESS* sees from the star and its companions/background stars at each pixel of each CCD. We produce it through our PRF model, which in turn requires the host star’s T_{eff} and apparent I_c . Over each image, the noise is computed for a range of possible aperture sizes about the brightest pixel (see S+15 Secs. 6.2 and 6.3), and then finally a single ‘noise’ for each transit is selected by choosing the aperture size that minimizes the noise.

2 Planet detection statistics

Using the planet detection model described in Sec. 1.4 and the target selection procedure of Sec. 1.5, we simulate three years of *TESS* observing, for six different possibilities for the third year: hemi, pole, hemi+ecl, ecl_long, ecl_short, and allsky. How many new planets do we detect, and how do their properties differ between Extended Missions?

2.1 Planet yield from the Primary Mission

We first examine our results for just the Primary Mission – the first two years of *TESS*’s observing. We follow with an analysis of our detected planet populations from a single Year-3 Extended Mission (Sec. 2.2), and then all six of our proposed Extended Missions (Sec. 2.3). Here we highlight commonalities and differences between S+15 and this work.

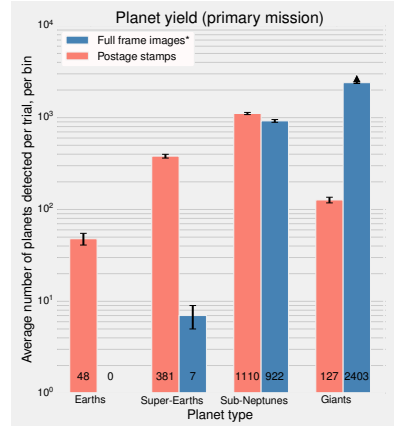


Figure 10: Mean numbers of planets detected in *TESS*’s Primary Mission (error bars are from Poisson fluctuations and do not account for systematic uncertainty). In postage stamp detections, the number of Earths ($R_p < 1.25R_{\oplus}$), super-Earths ($1.25R_{\oplus} \leq R_p < 2R_{\oplus}$), sub-Neptunes ($2R_{\oplus} \leq R_p < 4R_{\oplus}$) and giants ($R_p > 4R_{\oplus}$) is comparable to those quoted in Sullivan et al. [2015], despite modifications to our target selection procedure (Sec. 1.5). Our full frame images detections are complete for $R < 4R_{\oplus}$, and incomplete for giant planets. Here we disagree, by for instance two orders of magnitude in the super-Earth bin, with Sullivan et al. [2015] (see text).

Detected planet yield The first point of comparison is the detected planet yield from our simulation, shown in Fig. 10. The number of Earths, super-Earths, sub-Neptunes and giants we detect in postage stamps agrees with the numbers quoted by S+15, despite our modified target selection procedure. Other changes to our simulation’s inputs, for instance using an as-built model of *TESS*’s PSF informed by laboratory tests (courtesy Deborah Woods) rather than the idealized PSF described in Sec6.1 of S+15, also had little impact on this final result.

However, our yields from full frame images differ markedly from those quoted in Fig. 18 of S+15. We agree with S+15 that no Earths are detected in the full frame images. However, we detect only ~ 10 super-Earths by observing the 200,001st to 4,000,000th Merit-ranked stars at 30 minute cadence. This is two orders of magnitude less than the ~ 1000 super-Earth detections claimed from FFIs by S+15. There is also a discrepancy in FFI-detected sub-Neptunes, for which our current simulations predict that ~ 1000 will be detected, while S+15 predicted ~ 2000 .

We empirically verified that our full frame image detections are complete for $R < 4R_{\oplus}$ by enlarging the number of stars observed at 30-minute cadence and seeing that the number of detected planets with radii less than Neptune did not change. We do not understand the origin of the difference between our method and S+15’s, even after corresponding with P. Sullivan, but note that our results are in much better agreement with order-of-magnitude analytic arguments for *TESS*’s expected planet yield. Assuming an exponentially distributed stellar population in the galaxy and computing limiting magnitude thresholds, Winn [2013b] predicted detections of 600 – 6000 Neptunes, 24 – 300 super-Earths, and 1 – 10 Earth-sized planets, where the lower bounds correspond to planets detected with $\text{SNR} > 10$, and the upper bounds $\text{SNR} > 7$. S+15’s prediction of a total of 1500 detected super-Earths is a factor of 5 larger than these analytic estimates, while ours is in much better agreement.

Another plausibility argument that our current treatment of the FFIs is delivering more accurate results than the code employed by S+15 is that starting from the same input distribution of planets, we find a more reasonable detection bias against small planets. One should expect that the detection bias against small planets is a steep function of radius, given that $\delta \propto R_p^2$. S+15 predicted the detection of roughly twice as many sub-Neptunes as super-Earths; our current result has the ratio closer to 5-to-1 which seems more realistic.

Properties of planets detected in Primary Mission We show the population properties of planets detected in postage stamps and full frame

images during the Primary Mission in Figs. 12 and 13. In terms of the apparent planet radii R_p , orbital periods P , host star brightness, and host star T_{eff} , we agree with the results of S+15 for the planets detected in postage stamps. For instance, the dearth of $P < 5$ day Neptune-radius planets in Fig. 12 was observed by *Kepler* [Mazeh et al., 2016], and thus it is present in our input occurrence rates, rather than being an observational bias. It was also seen by S+15.

The differences between planets detected in postage stamps vs. in full frame images follow our expectation from our Merit statistic. Namely, Fig. 13 shows that at a fixed brightness, full frame image detections tend to occur at larger stellar effective temperature (and thus stellar radius). At a fixed host star radius, postage stamp detections occur around brighter stars.

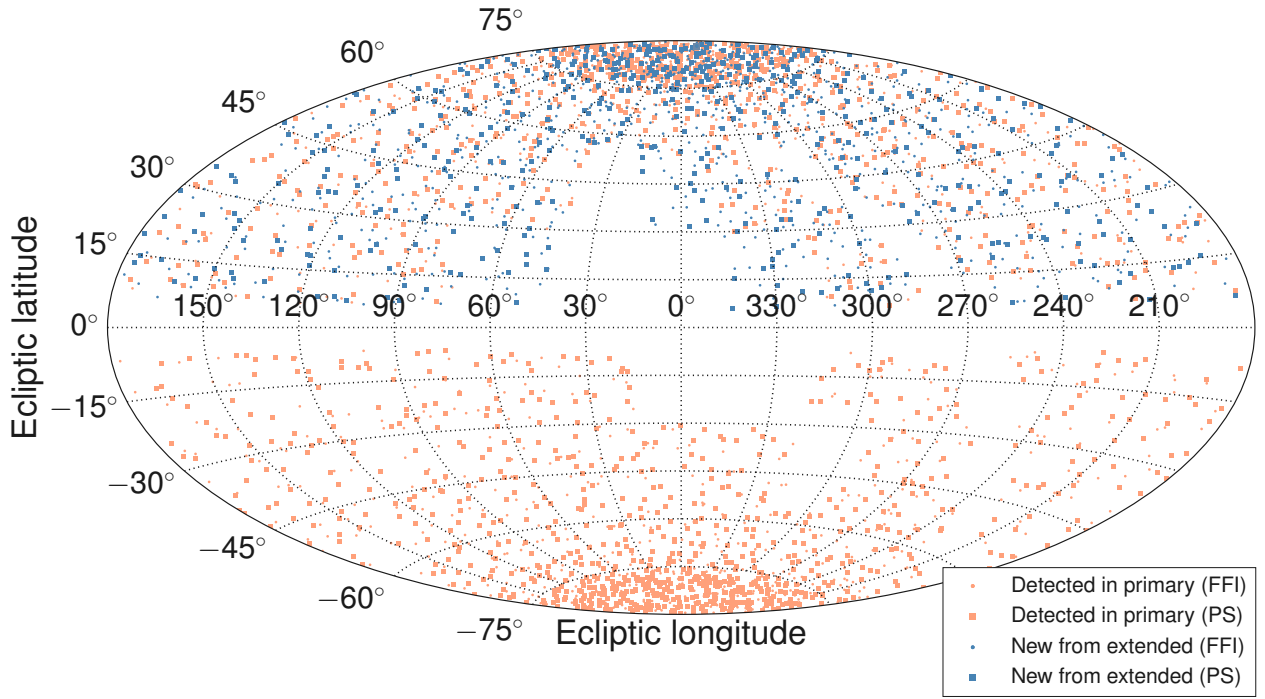
Impact of earth and moon crossings on Primary Mission’s detected planet yield During the Primary Mission, of the four cameras Camera 1 (closest to the ecliptic) suffers the most from earth and moon crossings. As noted in Table 1, we remove 4 of its 13 ‘observing sectors’. This reduces the number of planet detections near the ecliptic, and is visible in the orange points of Fig. 11. In the Primary Mission *TESS* detects ~ 20 planets with $R_p < 4R_{\oplus}$ from both 2 minute and 30 minute data in each $24^\circ \times 24^\circ$ camera field nearest to the ecliptic (where each field is observed for 2 *TESS* orbits). As implemented in our simulation, Earth and Moon crossings result in fields simply not being observed, so in these cases planets orbiting stars in these fields are never detected. Considering only the Primary Mission, we would naively expect that dropping a total of 9 fields over the two years (again, see Table 1) would result in a loss of $\sim 9 \times 20 = 180$ planets. This agrees with what our simulations actually give: running them without accounting for Earth and Moon losses returns a mean of 2678 detected planets with $R_p < 4R_{\oplus}$, while running them with Earth and Moon crossings gives a mean of 2482 such planets (a loss of 196 planets; 7% of the sub-Neptune yield).

2.2 Planet yield from an example Extended Mission: hemi

Before comparing our six selected Extended Mission scenarios simultaneously (Sec. 2.3), we describe the detected planet populations from a single realization of an Extended Mission. As an example case, we choose the hemi scenario.

A sky map showing the positions of detected planets for this mission is drawn in Fig. 11. Commenting on this map, we note that:

- Any planet detected in this scenario’s Primary Mission is also detected in its Extended Mission. We consequently color the de-



tected planets depending on if they are discovered in the Primary Mission, or whether they are detected only by virtue of the extra data collected in the Extended Mission. In our simulation, these extra observations will lead to new detections (a) because of an increased number of observed transits leading to a higher phase-folded SNR, which causes the transiting object's SNR to clear our threshold of 7.3, and/or (b) because raising the number of observed transits clears the minimum number of transits we require for detections ($N_{\text{tra}} \geq 2$).

- The ‘dropped’ fields described in Sec. 1.6 owing to Earth and Moon crossings are visible for both the Primary and Extended Missions in the $\lambda = (30^\circ, 0^\circ, 330^\circ, 300^\circ)$ fields.

In addition to examining the positions of the detected planets, we select and plot some of their key properties: planet radius R_p , orbital period P , apparent magnitude I_c , and effective temperature T_{eff} . See Figs. 12 and 13. Both of these figures are visualizations from a single Monte Carlo realization of the hemi scenario, and only show planets with $R_p < 4R_\oplus$. These plots clarify a few points:

- At a fixed period, Extended Missions help us detect smaller plan-

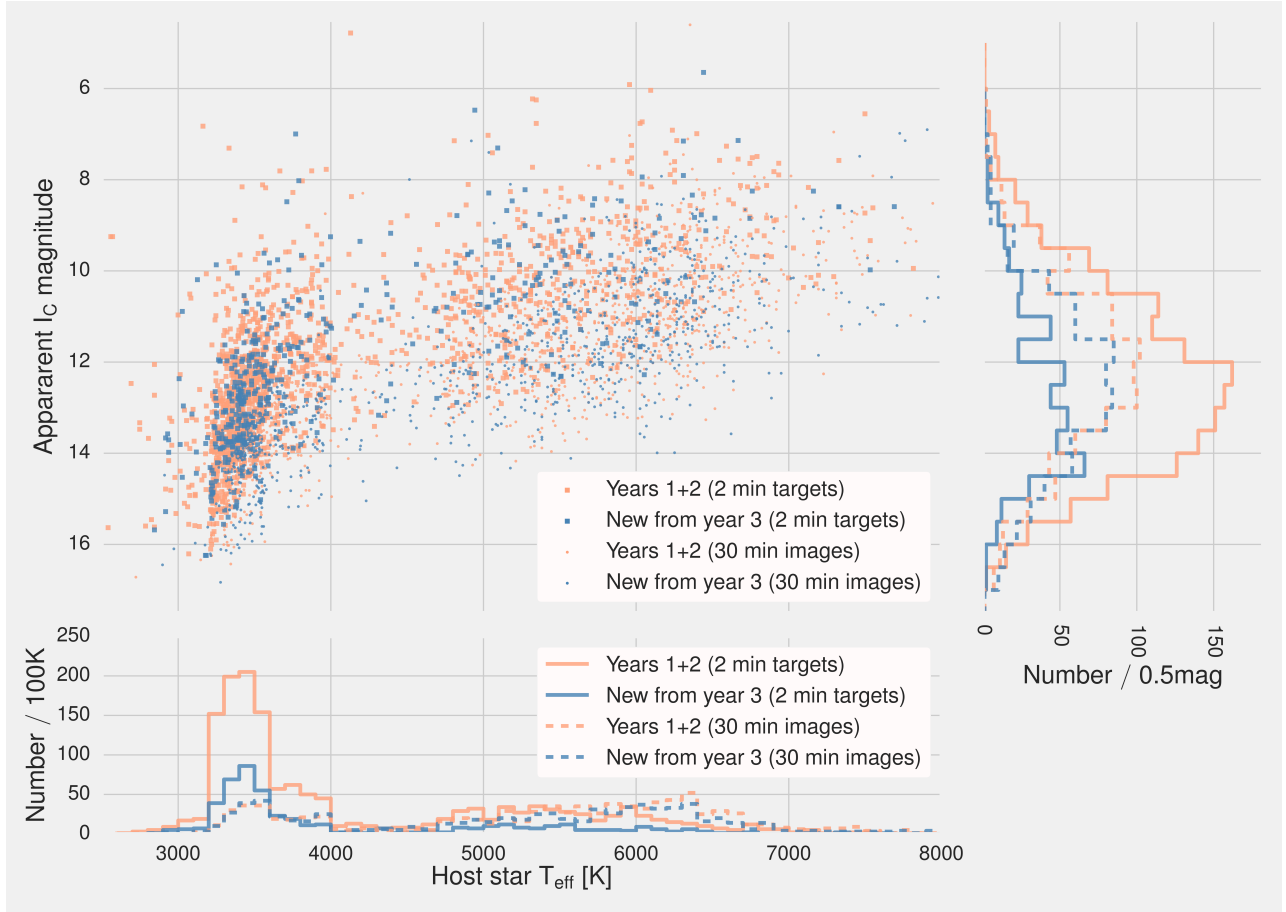
Figure 11: Positions of $R_p < 4R_\oplus$ planets detected in the hemi scenario. Squares (postage stamps) and dots (full frame images) are observed at 2 and 30 minute cadence respectively. Orange denotes detection over the first two years of observing (the Primary Mission), and blue denotes newly detected planets from the extra third year. The ‘gaps’ in fields due to Earth and Moon crossings during the Primary and Extended Missions are noted in Table 1. For instance, the field centered at $(\lambda = 330^\circ, \beta = 18^\circ)$ is observed in the Extended but not the Primary Mission.



ets; at a fixed radius, they let us probe out to longer periods. This is one of the major reasons to extend *TESS*'s observations.

- Almost all $R_p < 2R_\oplus$ planets are detected in postage stamps, not full frame images. This is an indication that the top 2×10^5 Merit stars are a sufficient sample to detect most of the $R_p < 2R_\oplus$ planets that *TESS* can detect.
- Postage stamp detections are biased towards M dwarfs. Per Fig. 5, this is largely because our selection procedure chooses many M dwarfs.
- For a given effective temperature, full frame images detect planets about dimmer stars. Projecting the FFI detections onto apparent I_c magnitude (Fig. 13, right panel), the median brightness of stars with planets detected from FFIs is actually greater than the median brightness of planets detected from PSs. This is because these detections are about stars with radii that, on average, are greater

Figure 12: Radius vs period of detected $R_p < 4R_\oplus$ planets from one Monte Carlo realization of the hemi scenario. At a fixed period, Extended Missions help us detect smaller planets; at a fixed radius, they let us probe out to longer periods. The radius histogram, and the location of all dots (rather than squares) on the scatter plot show that almost all $R_p < 2R_\oplus$ planets are detected in postage stamps, not full frame images (also shown in Fig. 10).



than those from postage-stamp detections.

There are a few other statistics that are interesting for purposes of characterizing the value of this Extended Mission – how many new planets do we detect? How many are at long orbital periods? How many are in habitable zones? We respond to these questions in Sec. 2.3, in particular showing our detected planet yields in Fig. 14.

2.3 Comparing planet yields from all Extended Missions based on new planet detection metrics

To compare Extended Missions in terms of planet detection statistics, we focus on the subset of all detected planets that are *newly* detected from each Extended Mission. These may come from stars that were not observed at all in the Primary Mission (notably for scenarios such as `ec1_long`), or they may also come from transiting planets that were observed in the Primary Mission with $\text{SNR} < 7.3$, or from

Figure 13: Apparent Cousins I magnitude plotted against effective temperature for $R_p < 4R_\oplus$ planets detected from one Monte Carlo realization of the `hemi` scenario. Postage stamp (PS) detections are biased towards M dwarfs in part because of our selection procedure. For a given effective temperature, full frame images (FFIs) are taken of dimmer stars.

planets that were single-transiters in the Primary Mission (we require $N_{\text{tra}} \geq 2$) for detection. With this in mind, for each Extended Mission scenario we ask the following questions:

1. N_{new} : How many new planets do we detect?
2. $N_{\text{new},P>20d}$: How many of these new planets are at long orbital periods, for instance $P > 20$ days?
3. $N_{\text{new,HZ}}$: How many are in the habitable zone?
4. $N_{\text{sys,extra planets}}$: In how many systems in which at least one planet was detected during the Primary Mission do we find extra planets in the Extended Mission?
5. $N_{\text{new,atm}}$: How many new planets do we find that are amenable to atmospheric characterization (defined below by Eq. 4)?
6. $N_{\text{new,new stars}}$: How many of the new planets come from stars that were not observed in the Primary Mission, vs.
7. $N_{\text{new,SNR}\vee N_{\text{tra}}}$ stars that were observed, but either did not have enough transits or a high enough SNR to result in a detection?

For each Year-3 scenario, we compare these numbers to the corresponding numbers from the Primary Mission as well as to the other 5 scenarios for Year 3. We show the results of our simulations in Fig. 14. The first point to notice is that for all but one of the new planet detection metrics (N_{new} , $N_{\text{new},P>20d}$, $N_{\text{new,HZ}}$, $N_{\text{sys,extra planets}}$, $N_{\text{new,atm}}$, $N_{\text{new,SNR}\vee N_{\text{tra}}}$) the yields between Extended Missions vary by less than a factor of two. The exception is in $N_{\text{new,new stars}}$, in which ec1_long detects roughly twice as many planets orbiting never-before-observed stars as any other proposed mission.

The second point is on the absolute yields of new planets: postage stamp observations find $\mathcal{O}(500)$ new planets, relative to the Primary Mission’s $\mathcal{O}(1500)$. Full frame image observations find $\mathcal{O}(800)$ new planets, relative to the Primary Mission’s $\mathcal{O}(900)$. All Extended Missions find $\mathcal{O}(1300)$ new planets, relative to the Primary Mission’s $\mathcal{O}(2500)$. We discuss these results – the rough invariance of the number of new planets to different pointing scenarios, and the essential contribution of FFIs – further in point #1 below.

Skimming the bottom panel for which missions are highlighted in green when accounting for both PSs and FFIs, we see that pole and allsky are the ‘superlative-winning’ missions in terms of detected planet statistics: considering both PSs and FFIs, pole places top-2 in 5 of 8 relevant categories, and allsky does the same in 6 of 8. They both do well at maximizing the number of newly detected planets,

Target stars (2 min)	hemi	pole	hemi+ecl	ecl_long	ecl_short	allsky
N_{uniq}	2051	2219	2051	2114	2127	2130
N_{new}	499	616	482	530	472	584
N_{pri}	1544	1543	1547	1557	1552	1543
$N_{\text{new,P>20d}}$	137	153	119	118	108	176
$N_{\text{pri,P>20d}}$	214	210	213	216	215	216
$N_{\text{new,HZ}}$	102	108	101	95	94	128
$N_{\text{pri,HZ}}$	196	201	200	208	202	200
$N_{\text{sys,extra planets}}$	62	54	59	38	53	82
$N_{\text{new,atm}}$	11	7	19	19	21	17
$N_{\text{pri,atm}}$	97	102	100	99	104	98
$N_{\text{new,new stars}}$	29	37	70	193	110	20
$N_{\text{new,SNR}\vee N_{\text{tra}}}$	471	580	411	337	362	564

Full Frames (30 min)	hemi	pole	hemi+ecl	ecl_long	ecl_short	allsky
N_{uniq}	1716	1682	1762	1558	1574	1776
N_{new}	785	803	846	639	744	849
N_{pri}	940	939	938	947	933	931
$N_{\text{new,P>20d}}$	116	122	114	89	110	128
$N_{\text{pri,P>20d}}$	80	82	80	80	83	80
$N_{\text{new,HZ}}$	20	16	21	12	25	18
$N_{\text{pri,HZ}}$	9	8	9	9	8	9
$N_{\text{sys,extra planets}}$	9	7	9	5	7	10
$N_{\text{new,atm}}$	3	1	5	2	2	5
$N_{\text{pri,atm}}$	7	7	7	7	7	6
$N_{\text{new,new stars}}$	35	56	90	173	61	22
$N_{\text{new,SNR}\vee N_{\text{tra}}}$	750	747	755	466	682	827

Combined	hemi	pole	hemi+ecl	ecl_long	ecl_short	allsky
N_{uniq}	3767	3901	3813	3672	3701	3907
N_{new}	1284	1419	1327	1169	1216	1433
N_{pri}	2483	2482	2486	2504	2485	2474
$N_{\text{new,P>20d}}$	253	275	234	207	218	304
$N_{\text{pri,P>20d}}$	294	292	294	296	298	296
$N_{\text{new,HZ}}$	122	124	122	107	120	146
$N_{\text{pri,HZ}}$	205	210	209	217	210	208
$N_{\text{sys,extra planets}}$	71	65	67	44	61	92
$N_{\text{new,atm}}$	14	8	24	21	23	22
$N_{\text{pri,atm}}$	104	108	107	106	112	104
$N_{\text{new,new stars}}$	63	92	161	366	171	42
$N_{\text{new,SNR}\vee N_{\text{tra}}}$	1220	1327	1167	803	1045	1390

Figure 14: Detected planet metrics for six possible Extended Missions (values are means of 50 Monte Carlo realizations of our calculation, all for $R_p < 4R_{\oplus}$). Top: postage stamp detections, Middle: full frame image only detections, Bottom: sum of both. The best two scenarios for select statistics are highlighted in green.

N_{uniq} : number of unique planets detected over all 3 years. N_{new} : number of planets detected in year 3 that were not detected in years 1&2 (newly detected planets). N_{pri} : number of planets detected in the Primary Mission (years 1&2). $N_{\text{new,P>20d}}$: number of newly detected planets with orbital periods greater than 20 days. $N_{\text{pri,P>20d}}$: same as previous, but from the Primary Mission. $N_{\text{new,HZ}}$: number of newly detected planets satisfying $0.2 < S/S_{\oplus} < 2.0$ (approximate habitable zone). $N_{\text{pri,HZ}}$: same as previous, from the Primary Mission. $N_{\text{sys,extra planets}}$: number of systems in which extra planets are detected. $N_{\text{new,atm}}$: number of newly detected planets with SNR in transmission greater than (that of GJ 1214b)/2, as measured by JWST – see text. $N_{\text{pri,atm}}$: same as previous, from Primary Mission. $N_{\text{new,new stars}}$: number of newly detected planets that orbit stars that were not observed during the Primary Mission. $N_{\text{new,SNR}\vee N_{\text{tra}}}$: number of newly detected planets that were observed during the Primary Mission, but either (a) which had $\text{SNR} < 7.3$, a non-detection and/or (b) had $N_{\text{tra}} < 2$, and so would not be ‘detected’.

while also performing well at detecting long period planets, and thus planets in their stars’ habitable zones. allsky also has the largest number of systems in which extra planets are detected.

We now discuss each metric in more depth:

1. N_{new} : we detect about as many new planets in Year 3 as we de-

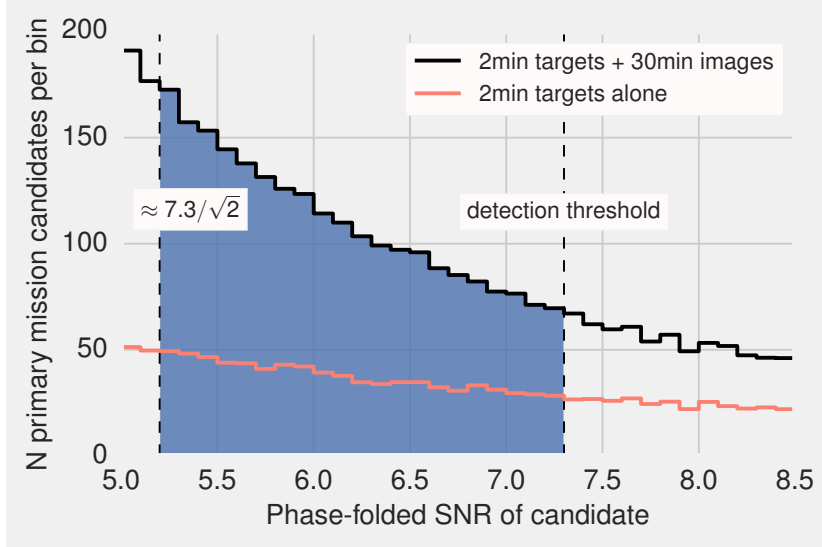


Figure 15: Histogram of phase-folded SNRs for candidate $R_p < 4R_{\oplus}$ planets following the Primary Mission (from both PS and FFI observations; values are means of 20 Monte Carlo trials; $N_{\text{tra}} \geq 2$). If an Extended Mission observes half of the sky, it roughly doubles the number of observed transits for half of the planets observed in the Primary Mission, enabling detection of $\approx 2316/2 = 1158$ planets (half of the blue integrated area in the plot). This coarse estimate is a similar result to our detailed calculations, and shows the value of continuing *TESS*'s observations irrespective of where we observe.

tect planets in either Years 1 or 2: roughly 1250. The worst and the best scenarios (`ecl_long` and `allsky`, respectively) differ only by a factor of 1.2. The fact that there are so many new planets to be detected from extended observations, particularly from full frame images, and that the absolute number of new planets is roughly invariant to the spacecraft's pointing, can be understood from Fig. 15. This figure illustrates a point that was originally noted by S+15: *TESS*'s Primary Mission will miss many short-period planets around bright stars, and is therefore incomplete even its intended hunting ground. For stars with $I_c > 9$, there are at least an order of magnitude more $R_p < 4R_{\oplus}$ transiting planets that *TESS* does not detect (Fig 22 of S+15). Our findings agree: there are a substantial number of planets just below the detection threshold, predominantly with $2R_{\oplus} < R_p < 4R_{\oplus}$ (Fig. 10). An Extended Mission will probe and detect this population, irrespective of where on the sky we observe. This result should hold equally well for realistic detection efficiency thresholds, and it demonstrates that extended observations will be valuable, because *TESS* will not yet be at the point of diminishing returns for longer observations (which will happen when more observations only allow pushing out to longer orbital periods). There will still be small, short-period candidates to discover after *TESS*'s Primary Mission.

2. $N_{\text{new}, P > 20\text{d}}$: it will be possible to detect as many new $P > 20$ day planets in one year of *TESS*'s Extended Mission as in both years of the Primary Mission. The Primary Mission detects about 295

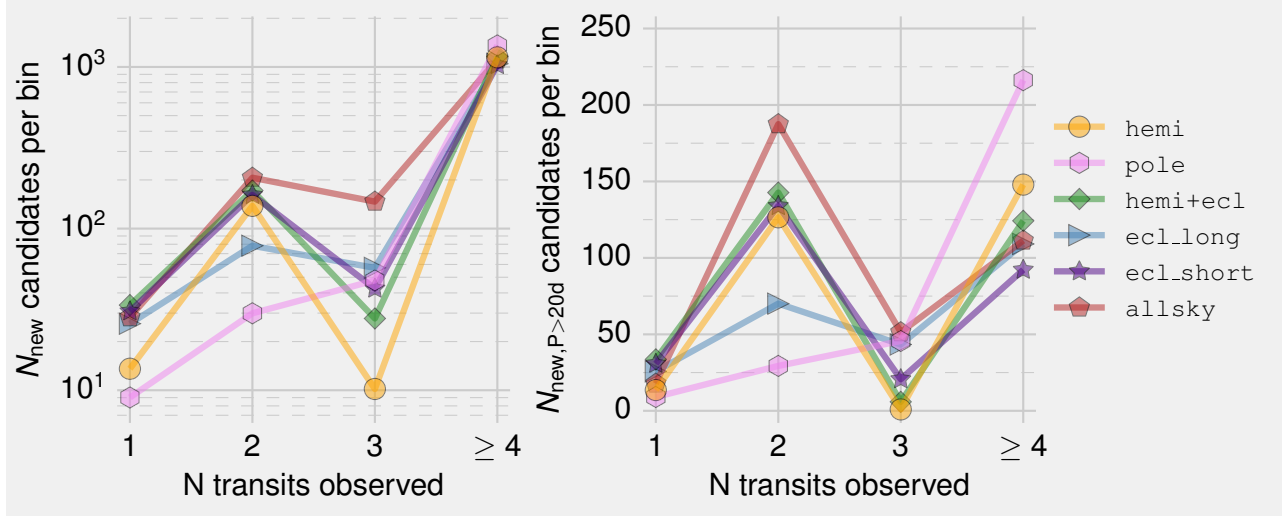
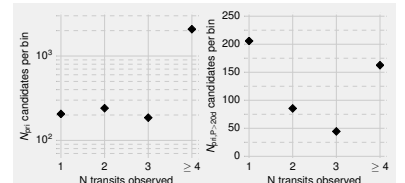


Figure 16: *Left:* Histogram of new $R_p < 4R_\oplus$ planet candidates from each Extended Mission as a function of the number of observed transits. Candidates are ‘detected’ in Fig. 14 if $N_{\text{tra}} \geq 2$. *Right:* Same as left, restricted to $P > 20$ day planets. If any given scenario has a ‘bump’ at 2 observed transits, then that scenario depends more heavily on our assumption of being able to make detections based on only two transits. Lines between points have no physical meaning; they are intended to improve readability.

such planets; `allsky` and `pole` scenarios detect similar amounts. These two scenarios are achieving the goal of long-period planet detection in slightly different ways: `pole` maximizes the average observing baseline per star, while `allsky` observes the greatest possible number of stars for longer than 40 days. The latter approach could succeed at detecting many planets (our result is that `allsky` detects the most $P > 20$ day planets), but it relies heavily upon the assumption that we can detect planets from only two transits over the course of the entire mission, even if this means only one transit in the Primary, and one transit in the Extended.

This point – that the ability of the `allsky` scenario to detect many long period planets is grounded on the assumption that two transits at high enough SNR are sufficient for detection – is made explicit in the right panel of Fig. 16. About half of the long period planets that `allsky` finds are detected with only two transits. By way of comparison, `pole` detects most of its long-period planets with ≥ 4 transits. This means that the `pole` detections are more secure. For two-transit detections, especially those separated by a gap of a year or more in the *TESS* data, it will be difficult to be confident in either the detection or in the derived orbital period. Experience from the *Kepler* mission showed that requiring 3 or more self-consistent transits substantially lowers the fraction of false signals [Burke et al., 2014]. In cases with a relatively high SNR per transit it is possible to confirm candidates, but with less certainty than if we had more transits in the first place.

3. $N_{\text{new,HZ}}$: we approximate the habitable zone as the geometric



shell around a host star in which a planet's insolation satisfies $0.2 > S/S_{\oplus} > 2.0$. With this approximation, the `allsky` scenario finds the most new habitable zone planets: 146 (which is subject to the same caveats discussed above for long period planet detections). The next-best scenarios, `pole`, `pole` and `hemi+ecl`, all detect around 120. Relative to the Primary Mission's 210 detections, this means Extended Missions boost the number of detected habitable zone planets by a factor of ~ 1.6 . For purposes of weighing the value of habitable-zone detections in deciding between missions, the result that these scenarios all detect a similar number of planets indicates that this metric will likely not 'tip the scales' in any direction.

We note in passing that $\sim 80\%$ of the habitable zone planets that *TESS* detects orbit M dwarfs with spectral classes ranging from M4 - Mo, and $\sim 15\%$ of them orbit M dwarfs later than M4. We show the relevant cumulative distribution in Fig. 18. Additionally, our values for the number of $0.2 < S/S_{\oplus} < 2$ planets from the Primary Mission are slightly revised from those of S+15: while S+15 found 48 ± 7 planets with $0.2 < S/S_{\oplus} < 2$ and $R_p < 2R_{\oplus}$, we find 34 ± 5 such planets. Adopting the habitable zone of Kopparapu et al. [2013], S+15 found 14 ± 4 planets with $R_p < 2R_{\oplus}$. We find 11 ± 3 such planets. The rule of thumb that Extended Missions give roughly $1.6 \times$ the number of new $0.2 < S/S_{\oplus} < 2$ habitable zone planets applies to the Kopparapu et al. [2013] habitable zone as well as $0.2 < S/S_{\oplus} < 2.0$. Another point raised by Fig. 19 is that the Kopparapu et al. [2013] habitable zone, which is physically motivated by 1-D radiative-convective cloud-free climate models with accurate absorption coefficients, results in roughly 3 times fewer 'habitable zone' planet detections than our ad-hoc criterion of $0.2 < S/S_{\oplus} < 2$.

4. $N_{\text{sys,extra}}$ planets: for how many systems do we detect extra planets? Our assumptions about multiple planet system distributions are crude – we assume independent probability draws from single planet occurrence distributions. Thus our simulated planet population does not have systems of tightly packed inner planets in realistic numbers. That said, we expect this statistic to be some indication of the information that we are not explicitly modeling, but which can be obtained from extended observations of planetary systems post-planet detection. This additional information includes improved precision on physical and dynamical parameters of the system. It also includes transit timing variations, which could be used to discover non-transiting planets as well as transiting outer companions. TTVs can also give dynamical hints for the

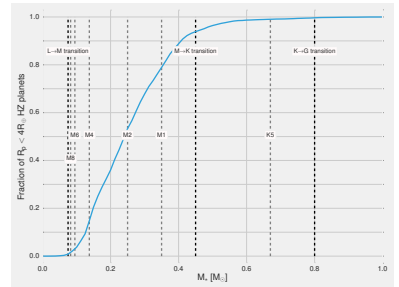


Figure 18: Cumulative distribution of $R_p < 4R_{\oplus}$ and $0.2 < S/S_{\oplus} < 2$ planet candidates from the Primary Mission (a proxy for the habitable zone). Boundaries of spectral classes are highly approximate, and taken from Habets and Heintze [1981] and Baraffe and Chabrier [1996].

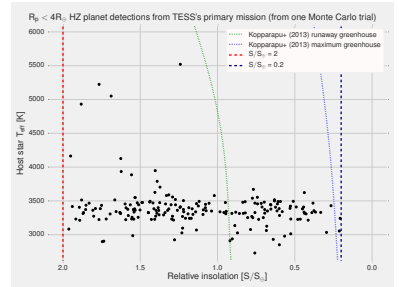


Figure 19: Scatter plot of $R_p < 4R_{\oplus}$ planet candidates falling in the S+15 or Kopparapu et al. [2013] habitable zones.

formation history of planetary systems, for instance, discriminating between *in situ* formation and inward migration as Mills et al. [2016] argued for the Kepler 223 system.

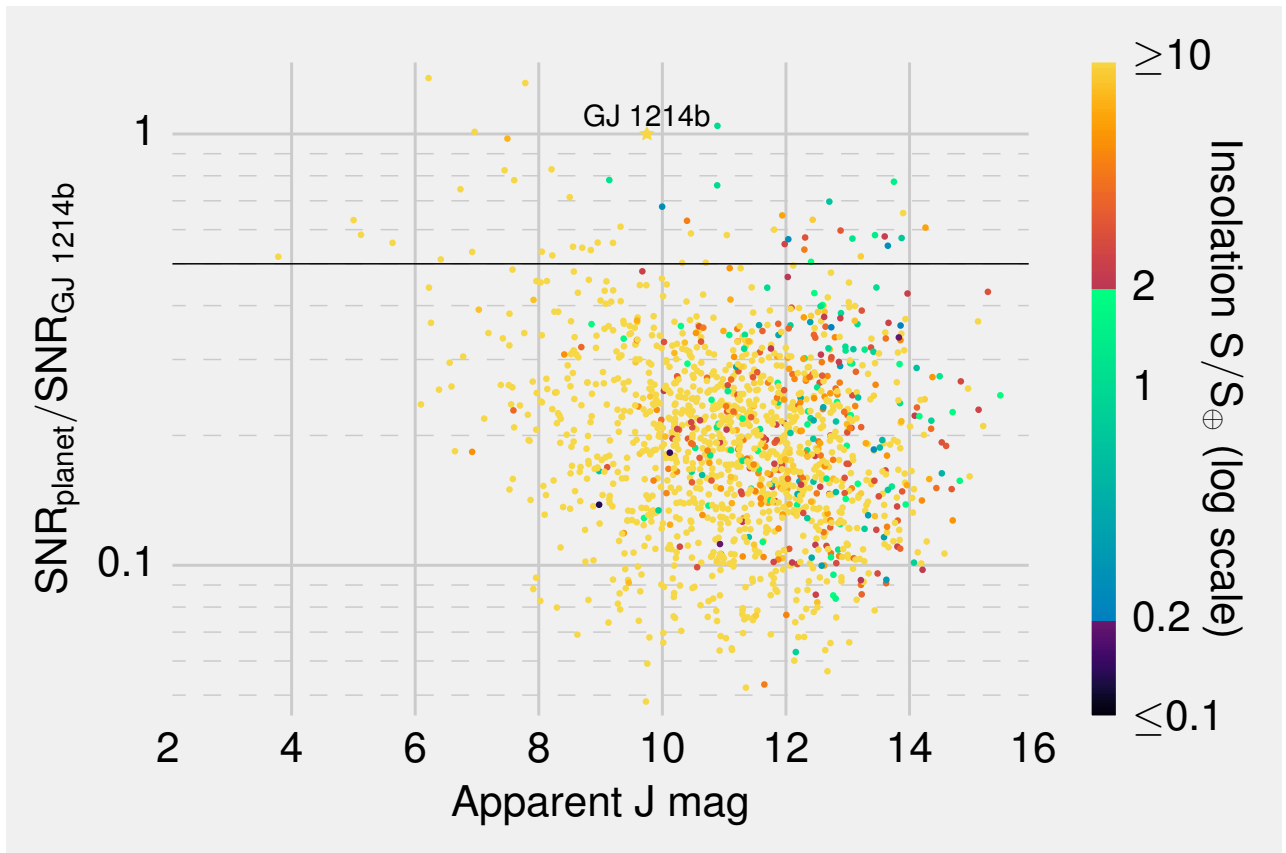
The most prominent feature in the results for this metric is that `ecl_long` detects the fewest systems with extra planets (44, which is 39% worse than the next-best). This is reasonable because `ecl_long` spends the most time looking at new sky, and in the process observes fewer systems that were detected in the Primary Mission. `hemi`, `hemi+ecl`, `pole`, and `ecl_short` all perform similarly, detecting ~ 65 such planets. `allsky` detects the most, at 92. While this is still subject to the assumption of two-transit recoverability, in this case the requirement is not too strong: only 10 of `allsky`'s systems with newly detected planets come from the case where the extra detected planet comes from two transits.

5. $N_{\text{new,atm}}$: We define ‘planets that are amenable to atmospheric characterization’ to mean planets whose SNR in transmission is at least half as large as that of GJ 1214b. We chose “at least half as large” rather than “equal to” in order to give a sufficiently large sample to prevent Poisson fluctuations from hindering our comparisons. The relevant signal in transit spectroscopy is the ratio of the areas of atmosphere’s annulus to the star’s disk on the sky plane, $\delta_{\text{atm}} = 2\pi R_p h_{\text{eff}} / (\pi R_\star^2)$, where the effective scale height of the atmosphere h_{eff} is proportional to the actual scale height. Assuming that the planet is in thermal equilibrium with incident radiation from the host star, and that its atmosphere has known mean molecular weight and Bond albedo, we can compute a representative signal. The noise performance depends on the observing instrument, and could be complex if not simply dominated by shot-noise from IR photons. We circumvent such complexities via an empirical formula provided to us by Drake Deming, based on a multi-variate regression fit to detailed simulations performed by Dana Louie. This formula estimates the SNR in transmission from 4 transits observed with JWST’s NIRISS instrument:

$$\begin{aligned} \log_{10} \text{SNR} = & 2.98 \log_{10} \left(\frac{R_p}{R_\oplus} \right) - 1.019 \log_{10} \left(\frac{M_p}{M_\oplus} \right) \\ & - 1.459 \log_{10} \left(\frac{R_\star}{R_\odot} \right) - 0.249 \log_{10} \left(\frac{a}{\text{AU}} \right) \\ & - 0.147(V - 5.0) + 0.193 \end{aligned} \quad (4)$$

for V the host star’s apparent V -band magnitude (calibrated for $3 > V > 22$), R_p the planet radius, M_p the planet mass, R_\star the star radius, and a the planet’s semi-major axis. The coefficients are physically sensible: the 2.98 coefficient of R_p minus

the 1.019 coefficient of M_p implies that the SNR depends inversely as bulk density, with puffier planets giving higher SNR for transit spectroscopy. Although this formula uses a V band magnitude ($\sim 0.5 - 0.6\mu\text{m}$), while NIRISS's SOSS mode covers $0.6 - 2.8\mu\text{m}$, the only difference if we were to use J band magnitudes would be in the coefficients preceding the stellar radius and the semi-major axis terms (and thus implicitly, in the stellar mass). Focusing our analysis to a SNR measured by *JWST* is sensible given *TESS*'s role as a 'JWST finder scope' [Deming et al., 2009]. We focus specifically on NIRISS given that it will likely be the workhorse *JWST* instrument for transmission spectroscopy [Béichman et al., 2014].



Reference parameters for GJ 1214b are those quoted by Charbonneau et al. [2009]: $R_p = 2.678R_\oplus$, $M_p = 6.55M_\oplus$, $R_\star = 0.211R_\odot$, $a = 0.0144\text{AU}$, $V = 15.1$. Using Eq. 4, we compute the SNR in transmission for all detected planets, for all Extended Mission scenarios. Fig. 20 shows one realization of the resulting distribution for planets detected in all three years of the pole scenario.

Figure 20: Scatter plot showing the SNR in transmission of detected planets with $R_p < 4R_\oplus$ from one Monte Carlo realization of all 3 years of the pole scenario. The SNR is computed from Eq. 4. Planets above the horizontal black line ($\text{SNR}_{\text{planet}} / \text{SNR}_{\text{GJ } 1214\text{b}} = 0.5$) are counted for Fig. 14's metric of planets with 'good' atmospheres for transmission spectroscopy. GJ 1214b is marked with a star. The coloring of planets indicates their relative insolation, as well as whether they fall our ad-hoc habitable zone ($0.2 < S/S_\oplus < 2$).

TESS mostly detects strongly irradiated planets (most points on Fig. 20 are yellow). A very small number, $\lesssim 10$, are both in the approximate habitable zone and also ‘favorable for atmospheric characterization’. Of course, a highly compelling target with lower SNR in transmission per transit might merit a more ambitious *JWST* observing program. We note that all of these planets are assumed to have identical mean molecular weights and cloud properties.

More importantly, Fig. 14 shows that most of the planets with atmospheres that are best for transmission spectroscopy are already discovered after two years. The best Extended Missions (`hemi+ecl`, `ecl_long`, `ecl_short` and `allsky`) boost the yield of such planets from ~ 100 to ~ 125 . The worst, `pole`, finds about an additional 10. This best-case boost of $1.25 \times$ more ‘good’ planets for atmospheric characterization is less than the relative boost of $1.6 \times$ more newly detected long period planets. Put differently, among the various possibilities for the Extended Mission, there is more variation in $N_{\text{new},P<20d}$ than in $N_{\text{new,atm}}$.

6. $N_{\text{new,new stars}}$: Intuitively we expect that to maximize the number of planets detected around “new” stars (those which were not observed during the Primary Mission) we should collect as many photons as possible from new stars. And the region on the sky with the greatest number of new stars is the ecliptic. It is not surprising, then, that the `ecl_long` scenario finds the largest number of planets around new stars. The `ecl_long` scenario dedicates 7 of a single year’s 13 observing sectors to the ecliptic (where the other 6 are spent centered at the North Ecliptic Pole due to excessive Earth and Moon crossings). It consequently detects twice as many new planets about newly observed stars as the next-best scenarios: `ecl_short` and `hemi+ecl` (366 vs 171 and 161, respectively). These latter two options also spend time observing the ecliptic, but with only one camera, rather than with all four cameras simultaneously. We note that even though `ecl_long` is the scenario most successful in detecting planets about new stars, the new stars represent only $\sim 30\%$ of the total number of new detections.¹⁰
7. $N_{\text{new,SNR}\vee N_{\text{tra}}}$: This statistic is the number of newly detected planets that are detected either (a) due to their final SNR clearing our threshold (logical) or (b) their number of observed transits being greater than or equal to 2. It is the complement to $N_{\text{new,new stars}}$: scenarios like `hemi`, `pole`, and `allsky` that do not observe many new stars will detect all of their planets from a boosted SNR and/or clearing the minimum transit threshold.

¹⁰ Here, we remind the reader that “new” refers only to *TESS* observations. Some of these stars will have been observed by K2 or other projects (see discussion in Sec. 3).

<code>hemi</code>	<code>pole</code>	<code>hemi+ecl</code>	<code>ecl_long</code>	<code>ecl_short</code>	<code>allsky</code>
162	154	190	167	183	198

Comment on meaning of ‘detected in postage stamps’ vs ‘detected in FFIs’
The invested reader may inquire “what about the cross-over case of planets that are observed as PSs during the Primary (Extended) Mission, but as FFIs in the Extended (Primary) Mission? These are not explicitly listed in Fig. 14”. When describing the entire unique planet population detected from Years 1-3, for simplicity of language we use ‘postage stamp detections’ to refer to planets that are observed at any time (Primary or Extended Missions) at 2 minute cadence. In these cases, the dominant contribution to the final signal to noise ratio tends to come from the PS observations. When describing new planet detections, we use ‘postage stamp detections’ to mean planets that were newly detected due to being observed as postage stamps in the Extended Mission. In other words, this ‘cross-over’ point only matters in discussions of the unique planet population from an entire mission, Years 1-3. Considering just the newly detected planet population, we can unambiguously specify whether the new detections came from full frame images or postage stamps, irrespective of their observations from the Primary Mission.

2.4 On the brightness of stars with detected planets

While `pole` does well by most metrics, a larger proportion of its newly detected planets orbit dim stars than the planet populations detected from alternatives like `allsky` or `hemi+ecl`. We demonstrate this in Fig. 21. The main point here is that if our only priority were to maximize the number of new detections around bright host stars, then `pole` would be the worst among the scenarios considered here. For instance, arbitrarily setting the bound at $I_c < 10$ and numerically integrating from Fig. 21’s data, we see in Table. 2 that there is a $\sim 30\%$ level difference between the missions. For point of reference, the Primary Mission detects 386 such planets – so a single year of Extended Mission detects roughly as many planets orbiting bright hosts as a single year of Primary Mission.

3 Discussion

3.1 Planning Year 3 with Years 4–N in mind

TESS’s orbit is stable, in principle, for more than 1000 years [Gangestad et al., 2013]. While minor mechanical failures should be expected on the timescale of a few years, it is plausible that the spacecraft

Table 2: Number of new, $I_c < 10$, $R_p < 4R_\oplus$ planets from each Extended Mission (average of 50 Monte Carlo realizations of our code; showing sum of PSs & FFIs). `pole` detects the fewest new planets orbiting bright stars.

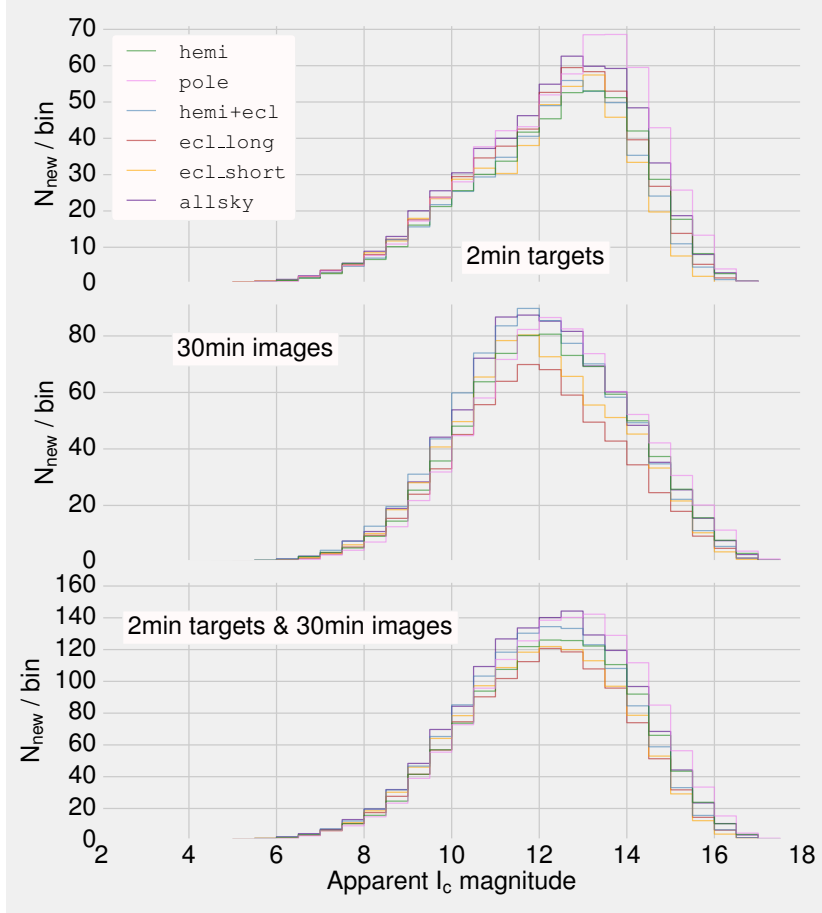


Figure 21: Histogram of apparent I_c magnitude of host star for newly detected $R_p < 4R_{\oplus}$ planets from all Extended Mission scenarios, for top: postage stamp detections, middle: full frame image detections, bottom: the sums thereof. While pole does well by most metrics, a larger proportion of the new planets it detects orbit dim stars compared to alternatives like allsky or hemi+ecl.

could outlive both the 2-year Primary Mission and the 1-year Extended Mission. Therefore, when choosing any particular plan for a 1-year Extended Mission, it makes sense to also consider the implications of an even longer Extended Mission.

A simple point is that hemi, pole, and hemi+ecl can all be inverted to their southern or northern complements for a fourth year of observing. This will yield a comparable number of new planets to what they find in year 3 ($\mathcal{O}(1300)$ with $R_p < 4R_{\oplus}$). This argues strongly to continue observing the entire sky, rather than focusing on a single ecliptic hemisphere after the Primary Mission’s completion. This would continue *TESS*’s role as a planet-discovery machine, while also addressing the practical matter of refining ephemerides in order to enable detailed characterization with suitable instruments.

The ecl_long, ecl_short, and allsky scenarios are less obviously extensible to multiple years. The main reasons to return to the ecliptic after performing ecl_long or ecl_short would be to make

TESS's survey truly 'all-sky', and to complete all possible K2 follow-up observations (see discussion below). Of course, this would need to happen during intervals in which the Moon and Earth were not in the way.

Any of our proposed scenarios could simply be repeated indefinitely, as could possible two-year Extended Missions in which our scenarios would be followed by their respective complement hemispheres. Slightly different trade-offs may arise when comparing two-year Extended Missions. For instance, consider: (1) two years of `allsky`; (2) repeating the Primary Mission for two years. If we repeat the Primary Mission over 2 years, the northern and southern CVZs each get 1 year of continuous observation. If we execute `allsky` for 2 years, the northern and southern 'long viewing zones' each get 2 years of 14-day windowed observations. The latter case allows 2-transit detections of $P \lesssim 1$ year planets over 2% of the sky. The former allows 2-transit detections of $P \lesssim 6$ month planets over 1% of the sky. This simple consideration of course misses that point that data obtained from repeating the Primary Mission would be less subject to aliasing problems and would have fewer period ambiguities. However repeating `allsky` for two years might be a middle ground between the two extreme strategies "repeat pole indefinitely" and "repeat the Primary Mission indefinitely".

A longer-term question is "when will *TESS* hit the point of diminishing returns?" The 'low-hanging fruit' of small planets transiting bright stars at short orbital periods will eventually be found if *TESS* continues to observe the same sky. The most important qualitative point of this memo, made in Fig. 15, is that after *TESS*'s Primary Mission there will be many objects remaining for which merely doubling the number of observed transits will enable their detection. Eventually though, the peak of the phase-folded SNR distribution shown in Fig. 15 will shift past the detection threshold, and more observations will only allow us to probe out to longer orbital periods and dimmer stars. No detailed study has yet quantified when *TESS* will reach this operating regime.

3.2 The ephemeris problem

Analytic motivation For follow-up observations, we will often need to predict future times of transits or occultations, ideally with an accuracy of an hour or less. After enough time has passed that the uncertainty has grown to a significant fraction of the orbital period, we say that the ephemeris has gone "stale," presenting a major obstacle to many follow-up programs. For *TESS*'s ground-based follow-up campaign, following up a planet with a stale ephemeris would re-

quire much more observing time for a successful result. Likewise, for planning space-based observations, for which observing time is always scarce, it is extremely important to have a reliable and precise ephemeris. For mass determination through the Doppler method, a stale transit ephemeris adds uncertainty to the planetary mass measurements, by increasing the number of effectively free parameters.

Consider then the problem of estimating $\sigma_{t_c}(T_x)$, the uncertainty of the mid-transit time σ_{t_c} for a given planet at some time T_x following its last-observed transit. We begin analytically: assume that the planet has $N_{\text{tra}} = 2$ observed transits, spaced an orbital period $P = 14$ days apart. Because that period is one half the nominal *TESS* dwell time of a given pointing, it represents the shortest period for which typically $N_{\text{tra}} = 2$, and as such is the worst-case scenario for predicting the times of future transits, amongst cases with $N_{\text{tra}} > 1$. Given two mid-transit times, each measured with the time's uncertainty σ_0 , separated by P , the uncertainty of a future mid-transit time can be derived by standard least-squares fitting and propagation of errors (e.g. Lyons [1991], Equation 2.18):

$$\sigma_{t_c}(T_x) = \sigma_0 \sqrt{1 + 2T_x/P + 2(T_x/P)^2} \quad (5)$$

Note that for observing future transits, $E \equiv T_x/P$ is an integer, and the above equation can be re-expressed:

$$\sigma_{t_c}(E) = \sigma_0 \sqrt{1 + 2E + 2E^2}, \quad (6)$$

which is bounded by the simpler approximation:

$$\sigma_{t_c}(E) \lesssim \sigma_0 (1 + \sqrt{2}E), \quad (7)$$

which is exact at $E = 0$, has a maximum 8% fractional error at $E = 1$, and becomes increasingly accurate as E increases. By $E = 20$, the fractional error of the latter approximation is less than 1%.

For $T_x = 2$ years and $P = 2$ weeks, then $E \approx 50$, so $\sigma_{t_c} \approx 75\sigma_0$. At 2-minute cadence, a typical value for the per-transit timing uncertainty is $\sigma_0 = 4$ minutes, and the predicted uncertainty on its mid-transit time is 5 hours two years later or 10 hours four years later. This leads to a simple rule of thumb:

For a two-transit super-Earth, the uncertainty in the predicted transit time, in hours, is numerically equal to about $2Y$, where Y is the number of years after the Primary Mission.

If the transits are observed only at 30-minute cadence, then uncertainty will be roughly 4 times greater: $\sigma_0 \sim 16$ minutes. This claim (“4× greater”) is based on Figure 9 of [Price and Rogers, 2014], a plot of the effects of finite cadence on timing precision. We compared the

precisions of 2-min and 30-min cadences for their specific example of $P = 10$ days and a dwell time of 1 month.

On the other hand, Fig. 17 shows that 7 in 8 of the planets detected by *TESS*'s Primary Mission will have $N_{\text{tra}} > 3$ and so their ephemerides should be better than the example derived analytically above. Rather than generalize the analytic equations, we resort to numerical simulations in order to predict the uncertainties of mid-transit times for planets expected to be discovered by *TESS*'s Primary Mission.

Numerical analysis We start with the analytic form Price and Rogers [2014] derive for the per-transit uncertainty on the mid-transit time σ_0 :

$$\sigma_0 = \frac{1}{Q} \sqrt{\frac{\tau T}{2}} \left(1 - \frac{t}{3\tau}\right)^{-1/2}$$

when $\tau \geq t$ and

$$\sigma_0 = \frac{1}{Q} \sqrt{\frac{t T}{2}} \left(1 - \frac{\tau}{3t}\right)^{-1/2} \quad (8)$$

when $t > \tau$, where Q is the SNR per transit, t is the cadence, T is the transit duration, and τ is the ingress (or egress) time. We have all the later terms from our yield simulation, and show the resulting distribution of σ_0 in Fig. 22. Indeed, our suggested σ_0 of about 4 minutes for postage stamps and 16 minutes for full frame images is reasonable, which is good because we computed the former from the $t \rightarrow 0$ limit of Eq. 8 originally derived by Carter et al. [2008].

Given the distributions on per-transit uncertainty of t_c , we then took an example planet with 4 transits. We drew “observed” mid-transit times from a Gaussian with zero mean and standard deviation σ_0 , and then ran a linear least squares regression. We then added just one data point 1 year after the final observed transit, and repeated the regression. This produces a cartoon-plot, Fig. 23, which confirms two expected points:

1. Years after the initial discovery, the uncertainty of mid-transit time is of order hours.
2. If we detect an additional transit 1 year after the final observed transit from the Primary Mission, the uncertainty on the mid-transit time decreases by an order of magnitude.

We proceed by repeating the above procedure for every planet, and evaluate typical 95% confidence intervals (“uncertainties”, loosely) for t_c , at typical times after the first transits, for all of our detected planets. Specifically, we take them at $T_x = 2$ and 4 years, and get Fig. 24. This figure confirms (top left panel) our analytic expectation that the uncertainty of mid-transit times in hours should

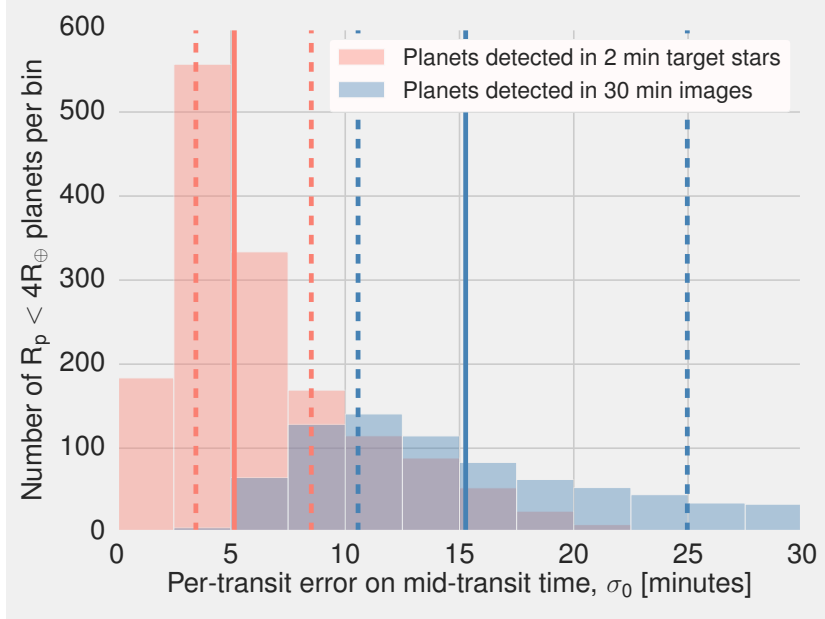


Figure 22: Uncertainty of mid-transit time on a single transit, σ_{tc} , for all detected $R_p < 4R_{\oplus}$ planets from the Primary Mission as computed from Eq. 8. Solid lines are medians, dashed lines are 25th and 75th percentiles.

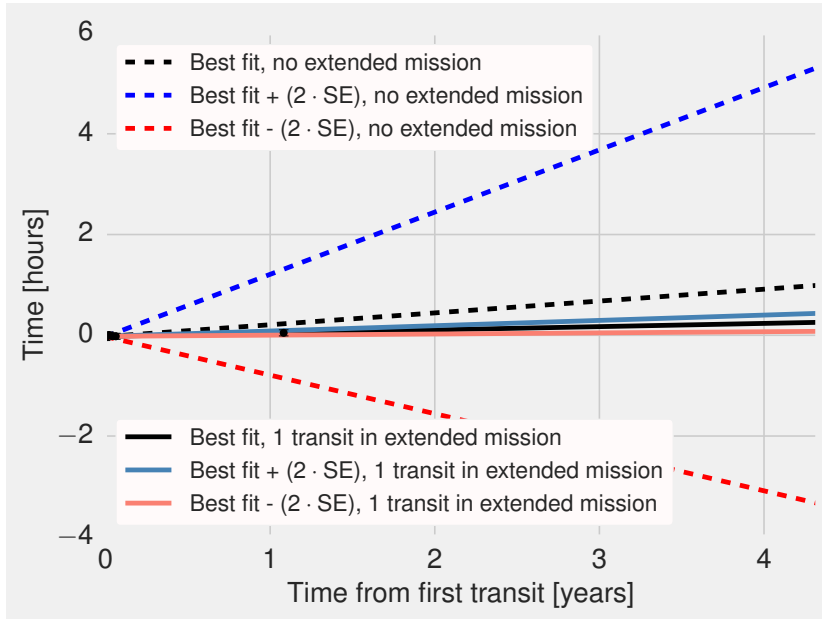


Figure 23: Observed mid-transit times (dots) and best fits to a linear ephemeris (lines). The dashed lines fit 4 data points from a nominal planet. The solid lines do the same, but with an additional transit observed one year later. ‘SE’ is the standard error on the slope which multiplied by 1.96 (rounded to 2 in the legend) gives a 95% confidence interval between the blue and orange lines.

be somewhat less than twice the number of years after *TESS* first observes the planet at 2-min cadence, since most such planets have $N_{tra} \geq 4$. It also confirms our rough expectation that the uncertainty on FFI mid-transit times is roughly 4 times that of postage stamps, although the uncertainties on FFIs have a much more uniform tail.



More importantly, Fig. 24 emphasizes the importance of refining *TESS*'s ephemerides: if we do not, the typical *TESS* planet will have many hours of uncertainty on its mid-transit time a few years following its detection. If we do follow-up, we will know when the planet transits to $\lesssim 1$ hour for many more years. This argues strongly for an Extended Mission which, whether over 1 or 2 years, re-observes many if not all of the targets that *TESS* detects in its Primary Mission. The smallest-radius Earths and super-Earths may otherwise be much more difficult to follow up, due to a stale ephemeris.

3.3 Risks and caveats

Risk that planet detection simulation gets yield wrong: What is the risk that we over or under-estimated *TESS*'s planet yield, either in the Primary Mission, or in any given Extended Mission? We summarized the assumptions that went into our yield calculations in Sec. 1.7.

Figure 24: Top row: histogram of 95% confidence intervals 2 (left) and 4 (right) years following the first detected transit in the Primary Mission. 20 minute bins. Bottom row: histogram of 95% confidence intervals 2 (left) and 4 (right) years following the first detected transit in the Primary Mission, but with an additional data point added to the analog of Fig. 23 one year after the transit in the initial time series (5 minute bins). Note that the top row's timescale is an order of magnitude greater than the bottom row. Solid lines are medians, dashed lines are 25th and 75th percentiles.

We made them believing that they were all good enough for useful relative comparisons of different sky-scanning scenarios, even if they are not correct in absolute terms to better than $\sim 50\%$.

Highlighting a few of these assumptions, in order of what we feel is decreasing concern:

- 1.) We assume no knowledge of the outcomes of prior transit searches.

As indicated in the text, this assumption is worst for the `ecl_long` and `ecl_short` scenarios, for which K_2 and *TESS*'s overlap will be important. Estimating the magnitude of our error, assume K_2 will have observed 70% of the sky in the $|\beta| < 6^\circ$ band about the ecliptic by 2019. Of the 1169 'new' $R_p < 4R_\oplus$ planets that *TESS* detects in `ecl_long`, 502 of them are within $|\beta| < 12^\circ$ of the ecliptic.

Assuming that all of these detections are uniformly distributed over the $|\beta| < 12^\circ$ band, this means that 35% (the ratio of the annuli) of *TESS*'s new planets will already have been detected in K_2 data. This simple estimate quantifies our global error in reporting 'new' planets near the ecliptic, but avoids the issue of merging the two datasets to discover long period planets. This latter opportunity could be an important reason to actually do `ecl_long` or `ecl_short` and thus demands detailed study, which we recommend below.

- 2.) The difference in $1.25R_\oplus < R_p < 2R_\oplus$ planet yield from S+15.

We discussed this point in Sec. 2.1. S+15 claim that *TESS* detects roughly 900 super-Earths in full frame images, and 500 in postage stamps. We claim that *TESS* detects roughly 10 super-Earths in full frame images, and 400 in postage stamps. This is a discrepancy of a factor of 4 in one of *TESS*'s most significant data products.

We do not understand the origin of the difference between our method and S+15's. That said, based on (a) raw output data generated by the author of S+15 and dated in May 2015 (3 months after initial ApJ submission, 1 month before acceptance); (b) the data we generated from the earliest available version of S+15's code, dated in October 2015 (before any of our methodological changes); (c) the analytic estimates of Winn [2013b] which predict ~ 300 super-Earth detections; and (d) a plausibility argument presented in Sec. 2.1 that showed S+15's results implied a detection efficiency biased sub-linearly in R_p , whilst ours implies a bias between linear and quadratic in R_p , we think that the current simulations give a more accurate picture.

- 3.) We use a SNR threshold of 7.3. This number was computed by S+15 based on the argument that it would be a sufficient threshold to give one false positive per 2×10^5 light curves. This

criterion is a self-consistent ad-hoc choice that we made for target stars. Applying the same criterion to full frame images would lead to more than one false positive, since full frame images come from a much larger sample of stars. Any pipeline that is written to work with *TESS* data will confront this problem: processing 10^8 vs. 4×10^6 vs. 2×10^5 stars all require different false positive thresholds. Extrapolating from S+15’s Fig 15, a threshold sufficient to give 0.05 false positives per 2×10^5 light curves, or 1 false positive per 4×10^6 light curves (as from our full frame images), is roughly 7.5. Making the same ad-hoc estimate that S+15 did and multiplying by 1.03 for the expected drop in SNR from cosmic ray noise gives a SNR threshold of 7.7 for full frame images. Considering our Fig. 15 (and noting the black line is for the sum of postage stamp and full frame image detections), adopting a SNR threshold of 7.7 for FFIs would mean a loss of $\sim 30 \times 4 = 120$ planets over two years, or 60 of what we claim are ‘detected planets’ from full frame images in 1 year’s Extended Mission.

4.) We use synthetic stars from a single galactic model (TRILEGAL).

One check on the robustness of this model would be to compare with other galactic models like GALAXIA [Sharma et al., 2011] or a Besaçon model [Robin et al., 2003]. We have already done this using a simple analytic model by Winn [2013b], which agrees with our work to within a factor of two. We might eventually use the real star catalog that *TESS*’s Target Selection Working Group is assembling, but this would come with large uncertainties on stellar radii, effective temperatures, and companion fractions.

While we recommend that these broader checks be performed in future *TESS* yield calculations, they are excessive for the purposes of this report given that we only used the nearest, brightest, stars ($d \lesssim 1\text{kpc}$, $I_c \lesssim 16$) with a simple prescription for background contamination in evaluating *TESS*’s $R_p < 4R_{\oplus}$ detections. The relative uncertainties become much greater if we try to estimate detections of giant planets and false positives throughout the galactic disk. That said, we take S+15’s cross-checks (cf Fig. 5 of that paper) against actual surveys of the local stellar population as indicative that we probably have the number of nearby stars, as well as their properties, correct to the absolute precision required for this work.

5.) At least 2 transits for detection: recall Figs. 16 and 17. If we were to use a more stringent criteria, for instance at least 3 transits for detection as the *Kepler* pipeline currently does, we would lose $\mathcal{O}(200)$ of the planets detected in the Primary Mission, and $\mathcal{O}(100)$ from the Extended Missions. This assumption disproportionately

affects long-period planets.

- 6.) We neglect instrument aging, spacecraft systematics, etc. To our best knowledge detailed models do not currently exist for how *TESS*'s optics and CCDs will degrade with time. We are also assuming that, as with *K2*, time-correlated spacecraft level systematics can be removed in post-processing. These assumptions are reasonable at our current state of pre-flight knowledge, and will need to be changed accordingly as the mission progresses. If we were to assume a gradual decline in photometric performance, for instance from an increased number of dead or 'hot' pixels, the relative Extended-Mission-to-Extended-Mission comparisons would remain identical. The absolute Extended-Mission-to-primary-Mission yields would decrease.
- 7.) We do not consider the efficacy of processing pipeline. For instance, *allsky* will come with period ambiguities and aliasing problems imposed by its 14 day sampling at the 'continuous' viewing zones. Similar issues are generic across Extended Missions for which we detect a small number of transits in the Primary Mission, and then a small number of transits in the Extended Mission.

A robust way to approach this problem would be to generate a synthetic simulated *TESS* dataset, *i.e.*, at the image-level, rather than at the idealized phase-folded SNR level from this work, for each Extended Mission's observations. Then actually perform astrometry on injected stars, extract light curves, de-trend them, and find their transits. This exercise would likely also be a useful way to prepare the SPOC and broader community for what we expect the era of *TESS* photometry to entail in terms of data quality.

Miscellaneous risks To be considered as knowledge of *TESS*'s in-flight performance improves:

- What is the risk of not meeting 'threshold' science – essentially whatever goals the science team decides will be the main drivers for an Extended Mission?
- Is there a risk of excessive false positives, for instance from field crowding, from any particular Extended Mission? This is primarily an issue for fields near the galactic plane and bulge.
- Would any expected partial instrument failures make a certain observing scenario infeasible? (*à la K2*, for instance)

4 Concluding remarks and recommendations

This trade-study laid out technical requirements, science goals, opportunities, and risks relevant to observing with *TESS* after its first two years. The baseline science requirements for *TESS*'s Primary Mission are defined [Ricker et al., 2014], and an Extended Mission offers a chance to re-prioritize. Is securing *TESS*'s ephemerides more important than probing out to the longest period planets? Are the variations in absolute new planet yields, at $\lesssim 30\%$ between all the Extended Missions, more valuable than other desires and opportunities?

We leave these questions open for the community to discuss at the *TESS* Wiki¹¹.

4.1 Recommendations

Analyze target prioritization problem and decide whether or not to optimize target selection based on results. Planet occurrence rates are functionally dependent on a star's properties – should this affect which stars we give upgraded cadence? Is our proposed Merit statistic (Eq. 2) how we want to prioritize targets?

Optimize cadence: observing 4×10^5 target stars at 4 minute cadence, rather than 2×10^5 at 2 minute cadence, may improve prospects for transit detection. Ideally a metric would be devised that quantifies, for each star, how much *improvement* would result from observing at short-cadence versus long-cadence. We could then prioritize the stars for which short-cadence delivers the most significant benefit. For instance if the number of short-cadence stars could be greatly reduced with little effect on the planet detection statistics, then this would allow the FFIs to be returned at a higher cadence, which would likely be desirable.

Take steps to address the 'upgrading cadence' problem: if there is a likely transiting planet in full frame image data, upgrading the planet to short cadence in future observing sectors improves the probability and fidelity of detection.

Guest Investigator Office / TESS Science Office: solicit advice from experts in asteroseismology and variable-sky astronomy to understand how Extended Missions affect their science cases (*e.g.*, data throughput rates are particularly important for time-sensitive supernovae observations). More broadly, solicit community feedback during the process of defining the Extended mission. This may entail a call for white papers, comments on this report, or direct

¹¹ <https://spacebook.mit.edu/display/TESS/Extended+Missions>. Contact luke@astro.princeton.edu, copying imeister@mit.edu, for an account with editing rights.

proposals to the GI office. As exemplified in NASA's 2016 Astrophysics Senior Review, everyone benefits from the discussions generated by such community feedback [Donahue et al., 2016].

Decide (explicitly or implicitly) on weights between our proposed metrics.

Perhaps also brainstorm others – Sec. 1.3 gives a summarized list. Are the $\lesssim 30\%$ variations in absolute new planet yields more valuable than other desires or opportunities?

Simulate combining TESS and K2 data from ecl_long and ecl_short.

This is perhaps the most important qualitative difference between observing towards and away from the ecliptic. Would *TESS+K2* enable more discoveries out at long periods than alternatives? How many of the new planets that *TESS* detects on the ecliptic will actually be detected by *K2*? Is the value-added of combining datasets a compelling case compared with discovery?

Further topics for study: 1.) After how many years would the planet yield start to show steeply diminishing returns? Suppose, for example, the Primary Mission were repeated indefinitely. How much dimmer would the host stars of new planets be, in each year? Would the planets tend to be smaller? Would there be fewer of them? 2.) Study the limiting case of allsky for 2 years, vs Primary Mission repeat for 2 years, vs pole \times 2 for 2 years. The most interesting aspect here is the continuous viewing zones: 2 CVZs at 14-day sampling, vs. 2 CVZs at continuous sampling for one-year each, vs. 1 CVZ for full sampling over two years.¹²

¹² Our simplified perfect period extraction would miss challenges from the data processing.

Acknowledgements

We thank Peter Sullivan for his support in the early phases of this work and for helpful comments on our results. We also are grateful to Jack Lissauer for input regarding the value of observing *Kepler's* field with *TESS*. The *TESS* project provided the computing resources used in this work and Ed Morgan, Isaac Meister, and Kenton Philips provided the support to keep the machines running.

Facility: *TESS*

Software: matplotlib [Hunter, 2007], NumPy [Walt et al., 2011], SciPy [Jones et al., 2001], pandas [McKinney], JPL NAIF's SPICE library [Acton, 1996], and the IDL Astronomy User's Library [Landsman, 1995].

Resources: This research has made use of the NASA Astrophysics Data System and the NASA Exoplanet Archive. The NASA Exoplanet Archive is operated by the California Institute of Technology, under contract with the National Aeronautics and Space Administration under the Exoplanet Exploration Program. This paper also makes use of data collected by the Kepler mission. Funding for the Kepler mission is provided by the NASA Science Mission directorate.

Appendices

A Models relevant to Earth and Moon crossings



Figure 25: Lens hood suppression plotted against the angular offset to the Earth or Moon. This suppression factor is defined as the fraction of incident flux that is blocked by the spacecraft, sunshade, lens hood, or combinations thereof.

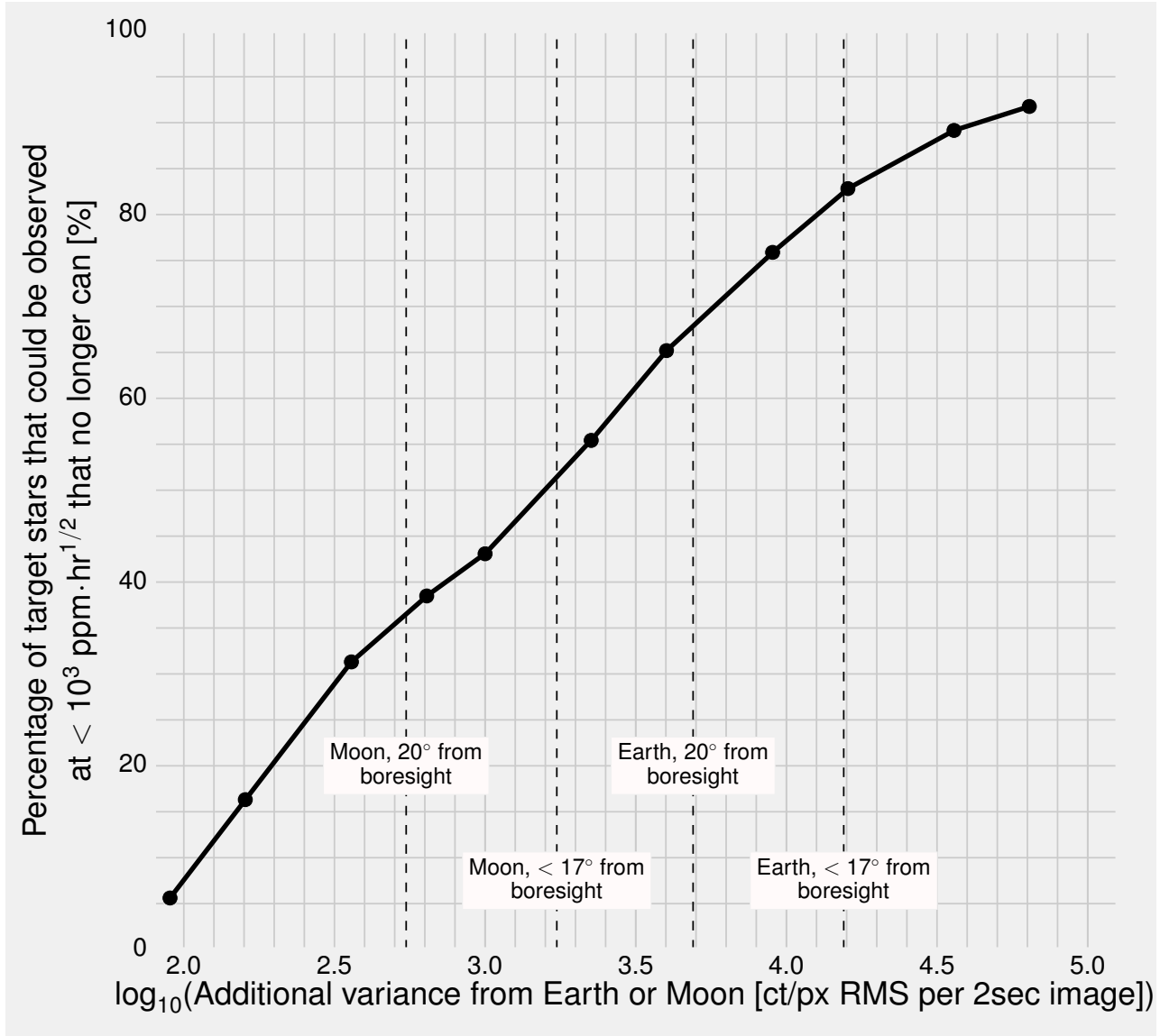


Figure 26: The procedure described in Sec. 1.6 drops fields in which <5% of the target stars which could be observed over 1 hour cannot be observed (only M dwarfs are affected). While this would apply to the cases with the Earth or Moon $\approx 28^\circ - 34^\circ$ from boresight, once closer, the effects become more serious. Lines between points guide the eye and are not exact.

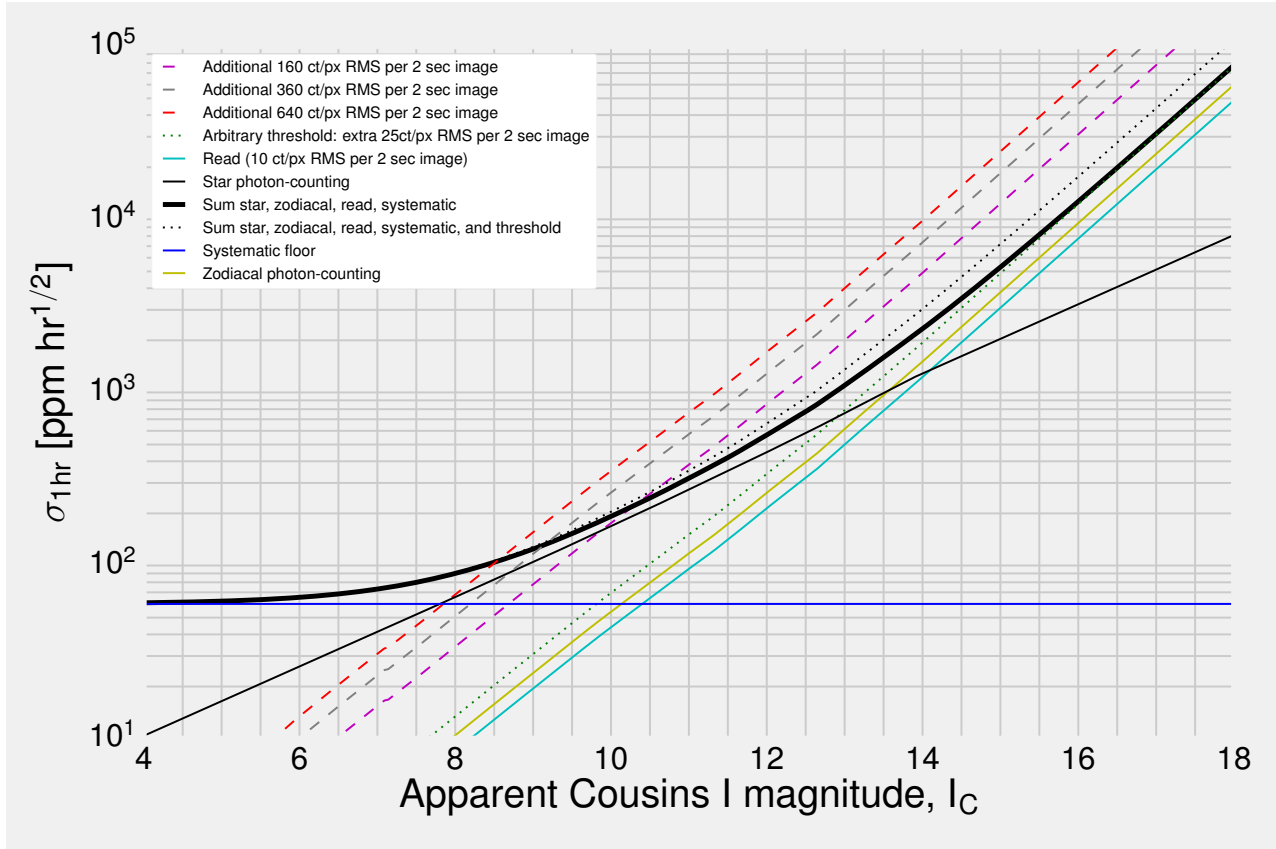


Figure 27: Same as Fig. 7, with threshold F_{thresh} of Sec. 1.6 overplotted (dotted green line). The expected noise budget is the thick black line; adding the threshold to it yields the dotted black line.

B Changes from Sullivan et al. [2015]

On the angular dependence of TESS’s pixel response function: In our SNR calculation, we do not keep track of individual times for every transit. How then do we assign PSFs to different transits from the same object that fall on different regions of the CCDs, and thus should have slightly better or degraded PSFs? (Largest cumulative flux fraction at the CCD’s center, smallest at the corners).

S+15 dealt with this by computing the mean of all the field angles (distance from the center of the CCD axis), and then passing this mean into a look-up table for PSFs based on four PSFs that had been computed from a ray-tracing model at four different field angles. S+15 then ‘observes’ each eclipsing object with a single class of PSF. This leads to the implausible phenomenon that extra observations can actually *lower* the SNR of an eclipsing object if they are taken with an unfavorable field angle/PSF. This effect is largely off-set by the extra pointing increasing the SNR, but for Extended Missions (coming back to the same objects at potentially very different field angles) it winds up reducing observed SNR for $\sim 3\%$ of detected objects.

In Extended Missions (as well as in the Primary Mission) we expect stars to land on very different regions of the CCD over the course of being observed. We simplify this in our work by assuming that all stars land on the center of the *TESS* CCDs (the green curve of S+15 Fig. 13). This assumption is justified because our chief point of quantitative comparison is the ability of different pointing strategies to impact *TESS*’s planet yield in Extended Missions, and there is little *a priori* reason to assume that any one pointing scenario should be biased for an extra amount of stars to land on the ‘bad regions’ of *TESS*’s CCDs.

References

- C. H. Acton. Planetary data system: Ancillary data services of NASA's Navigation and Ancillary Information Facility. *Planetary and Space Science*, 44(1):65–70, Jan. 1996. ISSN 0032-0633. DOI: 10.1016/0032-0633(95)00107-7. URL <http://www.sciencedirect.com/science/article/pii/0032063395001077>.
- I. Baraffe and G. Chabrier. Mass–Spectral Class Relationship for M Dwarfs. *The Astrophysical Journal*, 461(1), Apr. 1996. ISSN 0004637X. DOI: 10.1086/309988. URL <http://stacks.iop.org/1538-4357/461/i=1/a=L51>.
- G. Basri, L. M. Walkowicz, and A. Reiners. Comparison of Kepler Photometric Variability with the Sun on Different Timescales. *The Astrophysical Journal*, 769(1):37, 2013. ISSN 0004-637X. DOI: 10.1088/0004-637X/769/1/37. URL <http://stacks.iop.org/0004-637X/769/i=1/a=37>.
- C. Beichman, B. Benneke, H. Knutson, R. Smith, P.-O. Lagage, C. Dressing, D. Latham, J. Lunine, S. Birkmann, P. Ferruit, G. Giardino, E. Kempton, S. Carey, J. Krick, P. D. Deroo, A. Mandell, M. E. Ressler, A. Shporer, M. Swain, G. Vashtis, G. Ricker, J. Bouwman, I. Crossfield, T. Greene, S. Howell, J. Christiansen, D. Ciardi, M. Clampin, M. Greenhouse, A. Sozzetti, P. Goudfrooij, D. Hines, T. Keyes, J. Lee, P. McCullough, M. Robberto, J. Stansberry, J. Valenti, M. Rieke, G. Rieke, J. Fortney, J. Bean, L. Kreidberg, D. Ehrenreich, D. Deming, L. Albert, R. Doyon, and D. Sing. Observations of Transiting Exoplanets with the James Webb Space Telescope (JWST). *Publications of the Astronomical Society of the Pacific*, 126:1134–1173, Dec. 2014. DOI: 10.1086/679566.
- C. J. Burke, S. T. Bryson, F. Mullally, J. F. Rowe, J. L. Christiansen, S. E. Thompson, J. L. Coughlin, M. R. Haas, N. M. Batalha, D. A. Caldwell, J. M. Jenkins, M. Still, T. Barclay, W. J. Borucki, W. J. Chaplin, D. R. Ciardi, B. D. Clarke, W. D. Cochran, B.-O. Demory, G. A. Esquerdo, I. Thomas N. Gautier, R. L. Gilliland, F. R. Girouard, M. Havel, C. E. Henze, S. B. Howell, D. Huber, D. W. Latham, J. Li, R. C. Morehead, T. D. Morton, J. Pepper, E. Quintana, Darin Ragozzine, S. E. Seader, Y. Shah, A. Shporer, P. Tenenbaum, J. D. Twicken, and A. Wolfgang. Planetary Candidates Observed by Kepler IV: Planet Sample from Q1–Q8 (22 Months). *The Astrophysical Journal Supplement Series*, 210(2):19, 2014. ISSN 0067-0049. DOI: 10.1088/0067-0049/210/2/19. URL <http://stacks.iop.org/0067-0049/210/i=2/a=19>.

- J. A. Carter, J. C. Yee, J. Eastman, B. S. Gaudi, and J. N. Winn. Analytic approximations for transit light-curve observables, uncertainties, and covariances. *The Astrophysical Journal*, 689(1):499, 2008. URL <http://iopscience.iop.org/0004-637X/689/1/499>.
- D. Charbonneau, Z. K. Berta, J. Irwin, C. J. Burke, P. Nutzman, L. A. Buchhave, C. Lovis, X. Bonfils, D. W. Latham, S. Udry, R. A. Murray-Clay, M. J. Holman, E. E. Falco, J. N. Winn, D. Queloz, F. Pepe, M. Mayor, X. Delfosse, and T. Forveille. A super-Earth transiting a nearby low-mass star. *Nature*, 462(7275):891–894, Dec. 2009. ISSN 0028-0836, 1476-4687. DOI: [10.1038/nature08679](https://doi.org/10.1038/nature08679).
- D. Deming, S. Seager, J. Winn, E. Miller-Ricci, M. Clampin, D. Lindler, T. Greene, D. Charbonneau, G. Laughlin, G. Ricker, D. Latham, and K. Ennico. Discovery and Characterization of Transiting Super Earths Using an All-Sky Transit Survey and Follow-up by the James Webb Space Telescope. *Publications of the Astronomical Society of the Pacific*, 121(883):952, 2009. ISSN 1538-3873. DOI: [10.1086/605913](https://doi.org/10.1086/605913). URL <http://stacks.iop.org/1538-3873/121/i=883/a=952>.
- M. Donahue, M. Bautz, R. Green, G. Hasinger, L. Kaltenegger, H. Krawczynski, A. MacFayden, D. McCammon, R. Oppenheimer, P. Szkody, and D. Zaritsky. 2016 NASA Astrophysics Senior Review. Technical report, NASA, Feb. 2016. URL http://science.nasa.gov/media/medialibrary/2016/06/09/Main_Panel_SR2016_Report_FinalTAGGED.pdf.
- C. D. Dressing and D. Charbonneau. The Occurrence of Potentially Habitable Planets Orbiting M Dwarfs Estimated from the Full Kepler Dataset and an Empirical Measurement of the Detection Sensitivity. *arXiv preprint arXiv:1501.01623*, 2015. URL <http://arxiv.org/abs/1501.01623>.
- D. A. Fischer and J. Valenti. The Planet-Metallicity Correlation. *The Astrophysical Journal*, 622:1102–1117, Apr. 2005. ISSN 0004-637X. DOI: [10.1086/428383](https://doi.org/10.1086/428383). URL <http://adsabs.harvard.edu/abs/2005ApJ...622.1102F>.
- F. Fressin, G. Torres, D. Charbonneau, S. T. Bryson, J. Christiansen, C. D. Dressing, J. M. Jenkins, L. M. Walkowicz, and N. M. Batalha. THE FALSE POSITIVE RATE OF KEPLER AND THE OCCURRENCE OF PLANETS. *The Astrophysical Journal*, 766(2):81, Apr. 2013. ISSN 0004-637X, 1538-4357. DOI: [10.1088/0004-637X/766/2/81](https://doi.org/10.1088/0004-637X/766/2/81).
- J. W. Gangestad, G. A. Henning, R. R. Persinger, and G. R. Ricker. A high Earth, lunar resonant orbit for lower cost space

science missions. *arXiv preprint arXiv:1306.5333*, 2013. URL <http://arxiv.org/abs/1306.5333>.

L. Girardi, M. A. T. Groenewegen, E. Hatziminaoglou, and L. da Costa. Star counts in the Galaxy: Simulating from very deep to very shallow photometric surveys with the TRILEGAL code. *Astronomy and Astrophysics*, 436(3):895–915, June 2005. ISSN 0004-6361, 1432-0756. DOI: 10.1051/0004-6361:20042352. URL <http://www.edpsciences.org/10.1051/0004-6361:20042352>.

G. M. H. J. Habets and J. R. W. Heintze. Empirical bolometric corrections for the main-sequence. *Astronomy and Astrophysics Supplement Series*, 46:193–237, Nov. 1981. ISSN 0365-0138.

T. J. Henry, W.-C. Jao, J. P. Subasavage, T. D. Beaulieu, P. A. Ianna, E. Costa, and R. A. Méndez. The solar neighborhood. XVII. Parallax results from the CTIOPI 0.9 m program: 20 new members of the RECONS 10 parsec sample. *The Astronomical Journal*, 132(6):2360, 2006. URL <http://iopscience.iop.org/1538-3881/132/6/2360/205485.web.ps.gz>.

J. D. Hunter. Matplotlib: A 2d Graphics Environment. *Computing in Science & Engineering*, 9(3):90–95, 2007. ISSN 1521-9615. DOI: 10.1109/MCSE.2007.55. URL <http://ieeexplore.ieee.org/lpdocs/epic03/wrapper.htm?arnumber=4160265>.

J. A. Johnson, K. M. Aller, A. W. Howard, and J. R. Crepp. Giant Planet Occurrence in the Stellar Mass-Metallicity Plane. *Publications of the Astronomical Society of the Pacific*, 122(894):905, 2010. ISSN 1538-3873. DOI: 10.1086/655775. URL <http://stacks.iop.org/1538-3873/122/i=894/a=905>.

E. Jones, T. Oliphant, P. Peterson, et al. Open source scientific tools for python, 2001.

C. H. Kepner and B. B. Tregoe. Rational Manager. 1965. URL <http://agris.fao.org/agris-search/search.do?recordID=US201300461852>.

D. M. Kipping and C. Lam. Transit Clairvoyance: Enhancing TESS follow-up using artificial neural networks. Private communication, June 2016.

R. k. Kopparapu, R. Ramirez, J. F. Kasting, V. Eymet, T. D. Robinson, S. Mahadevan, R. C. Terrien, S. Domagal-Goldman, V. Meadows, and R. Deshpande. Habitable Zones Around Main-Sequence Stars: New Estimates. *The Astrophysical Journal*, 765(2):131, Mar. 2013. ISSN 0004-637X, 1538-4357. DOI: 10.1088/0004-637X/765/2/131. arXiv: 1301.6674.

W. B. Landsman. The IDL Astronomy User's Library. volume 77, page 437, 1995. URL <http://adsabs.harvard.edu/abs/1995ASPC..77..437L>.

L. Lyons. *A Practical Guide to Data Analysis for Physical Science Students*. Cambridge University Press, Nov. 1991. ISBN 978-0-521-42463-9. 1996 paperback reprinting.

T. Mazeh, T. Holczer, and S. Faigler. Dearth of short-period Neptunian exoplanets - a desert in period-mass and period-radius planes. *Astronomy & Astrophysics*, 589:A75, May 2016. ISSN 0004-6361, 1432-0746. DOI: [10.1051/0004-6361/201528065](https://doi.org/10.1051/0004-6361/201528065). URL <http://arxiv.org/abs/1602.07843>. arXiv: [1602.07843](https://arxiv.org/abs/1602.07843).

W. McKinney. pandas: a foundational python library for data analysis and statistics.

S. M. Mills, D. C. Fabrycky, C. Migaszewski, E. B. Ford, E. Petigura, and H. Isaacson. A resonant chain of four transiting, sub-Neptune planets. *Nature*, 533(7604):509–512, May 2016. ISSN 0028-0836. DOI: [10.1038/nature17445](https://doi.org/10.1038/nature17445). URL <http://www.nature.com/nature/journal/v533/n7604/full/nature17445.html>.

M. A. C. Perryman, L. Lindegren, J. Kovalevsky, E. Hoeg, U. Bastian, P. L. Bernacca, M. Crézé, F. Donati, M. Grenon, M. Grewing, F. van Leeuwen, H. van der Marel, F. Mignard, C. A. Murray, R. S. Le Poole, H. Schrijver, C. Turon, F. Arenou, M. Froeschlé, and C. S. Petersen. The HIPPARCOS Catalogue. *Astronomy and Astrophysics*, 323, July 1997. ISSN 0004-6361.

E. M. Price and L. A. Rogers. Transit Light Curves with Finite Integration Time: Fisher Information Analysis. *The Astrophysical Journal*, 794(1):92, Sept. 2014. ISSN 1538-4357. DOI: [10.1088/0004-637X/794/1/92](https://doi.org/10.1088/0004-637X/794/1/92). URL <http://arxiv.org/abs/1408.4124>. arXiv: [1408.4124](https://arxiv.org/abs/1408.4124).

G. R. Ricker, J. N. Winn, and R. Vanderspek. Transiting Exo-planet Survey Satellite. *Journal of Astronomical Telescopes, Instruments, and Systems*, 1(1):014003, Oct. 2014. ISSN 2329-4124. DOI: [10.1117/1.JATIS.1.1.014003](https://doi.org/10.1117/1.JATIS.1.1.014003). URL <http://astronomicaltelescopes.spiedigitallibrary.org/article.aspx?doi=10.1117/1.JATIS.1.1.014003>.

A. C. Robin, C. Reylé, S. Derrière, and S. Picaud. A synthetic view on structure and evolution of the milky way. *Astronomy & Astrophysics*, 409(2):523–540, 2003.

- S. Sharma, J. Bland-Hawthorn, K. V. Johnston, and J. Binney. Galaxia: a code to generate a synthetic survey of the Milky Way. *The Astrophysical Journal*, 730(1):3, Mar. 2011. ISSN 0004-637X, 1538-4357. DOI: 10.1088/0004-637X/730/1/3. URL <http://arxiv.org/abs/1101.3561>. arXiv: 1101.3561.
- P. W. Sullivan, J. N. Winn, Z. K. Berta-Thompson, D. Charbonneau, D. Deming, C. D. Dressing, D. W. Latham, A. M. Levine, P. R. McCullough, T. Morton, G. R. Ricker, R. Vanderspek, and D. Woods. THE TRANSITING EXOPLANET SURVEY SATELLITE: SIMULATIONS OF PLANET DETECTIONS AND ASTROPHYSICAL FALSE POSITIVES. *ApJ*, 809(1):77, aug 2015. DOI: 10.1088/0004-637X/809/1/77. URL <http://dx.doi.org/10.1088/0004-637X/809/1/77>.
- van Leeuwen and F. v. Leeuwen. Validation of the new Hipparcos reduction. *Astronomy & Astrophysics*, 474(2):12, 2007. DOI: 10.1051/0004-6361:20078357.
- S. v. d. Walt, S. C. Colbert, and G. Varoquaux. The NumPy Array: A Structure for Efficient Numerical Computation. *Computing in Science & Engineering*, 13(2):22–30, Mar. 2011. ISSN 1521-9615. DOI: 10.1109/MCSE.2011.37. URL <http://scitation.aip.org/content/aip/journal/cise/13/2/10.1109/MCSE.2011.37>.
- J. Wang and D. A. Fischer. Revealing a Universal Planet–Metallicity Correlation for Planets of Different Sizes Around Solar-type Stars. *The Astronomical Journal*, 149(1):14, 2015. ISSN 1538-3881. DOI: 10.1088/0004-6256/149/1/14. URL <http://stacks.iop.org/1538-3881/149/i=1/a=14>.
- J. N. Winn. Expected photon fluxes in the TESS bandpass. *TESS Science Memo No. 1, Version 2. Available upon request.*, 2013a.
- J. N. Winn. Number of Searchable Stars. *TESS Science Memo No. 5, Version 1. Available upon request.*, 2013b.